Marine and Petroleum Geology 158 (2023) 106528

Contents lists available at ScienceDirect

Marine and Petroleum Geology

journal homepage: www.elsevier.com/locate/marpetgeo

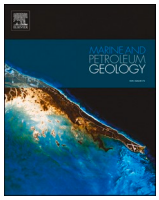

Variations and causes of *in-situ* stress orientations in the Dibei-Tuziluoke Gas Field in the Kuqa Foreland Basin, western China

Guoding Yu [a], Keyu Liu [a,*], Kelai Xi [a], Xianzhang Yang [b], Jing Yuan [a], Zhenping Xu [b], Lu Zhou [b], Shaoyong Hou [c]

[a] School of Geosciences, China University of Petroleum, Qingdao, Shandong, 266580, China
[b] Institute of Petroleum Exploration and Development, Tarim Oil Field, CNPC, Korla, 841000, China
[c] Oil & Gas Field Productivity Construction Department, Tarim Oil Field, CNPC, Korla, 8410001, China

ARTICLE INFO

Keywords:
Fractures
Borehole breakouts
Drilling-induced fractures
Stress variation
Stress rotation
Kuqa Foreland Basin

ABSTRACT

The Kuqa Foreland Basin, adjacent to the southern Tianshan Mountains, is an important gas-producing basin in northwestern China. The development of the basin is dominated by a regional stress field with orientations of the maximum horizontal stress (S_{Hmax}) in the north-south direction, as a result of the collision between the Indian and Eurasian Plates. Previous studies have noted variations in the stress state in the Kuqa Foreland Basin; however, little attention has been paid to understanding the mechanisms causing such variations. In this study, a systematic analysis of *in-situ* S_{Hmax} orientations and fractures has been carried out using image logs from eight wells and XMAC/DSI logs from five wells. These wells are located in an East-West (E-W) trending fold-thrust in the foreland basin. The S_{Hmax} orientations (having quality ranked between A and D) obtained from borehole breakouts and drilling-induced fractures are highly variable and occur as two evidently different stress patterns on a scale of less than 10 km. The first stress pattern with S_{Hmax} orientations between NNW and NNE (165.08 and 188.59 °N) is broadly comparable to the regional stress field inferred from earthquake focal mechanism solutions in northwestern China from the World Stress Map (WSM). The stress pattern is interpreted to be controlled by plate boundary forces related to the collision between the Indian and Eurasian Plates. The S_{Hmax} orientations for the second stress pattern, however, ranging from NNE to ENE (26.65–57.77 °N), are clearly inconsistent with the regional stress filed and have been influenced by local geological factors. Faults and hinge-parallel fractures (trending in an approximately W-E direction) formed during the syn-folding stage probably resulted in heterogeneity of elastic properties and thus deflected S_{Hmax} orientations, both laterally and vertically, to generate the second stress pattern. The NE-striking hinge-oblique fractures are interpreted to have formed in response to the stress reorientation. Observations in this study suggest that there may exist a close relationship between fracturing (faulting) and stress variations, and pre-existing faults and fractures can influence subsequent fracturing by regulating local stress fields on a scale of several kilometers. The coupling between fracturing or faulting and stress produced fracture swarms, which can significantly enhance fluid flow and hence petroleum production.

1. Introduction

Understanding the presence and extent of subsurface natural fractures and *in-situ* stress orientations of fractured reservoirs is important for petroleum production and fluid flow in the subsurface (Barton et al., 1995; Finkbeiner et al., 1997; Ju and Wang, 2018; Ganguli et al., 2018; Baouche et al., 2020, 2021). Stress magnitudes and directions in the upper crust, however, are extremely complicated due to the compositional and structural heterogeneities of geological bodies (Fossen, 2020). The stress orientation complexity arises mainly from the fact that geological factors at different scales (e.g. plate motion, topography, fault and fracture) can have significant impact on maximum horizontal stress (S_{Hmax}) orientations (Rajabi et al., 2016a). Continental scale S_{Hmax} orientations are observed to be generally aligned with the direction of plate motion, and the first-order stress pattern (>500 km) is considered to be controlled by forces applied at plate boundary (Zoback, 1992;

* Corresponding author.
E-mail addresses: guodingyu009@gmail.com (G. Yu), liukeyu@upc.edu.cn (K. Liu), kelai06016202@163.com (K. Xi), yangxztlm@petrochina.com.cn (X. Yang), drjyuan@163.com (J. Yuan), xuzenp-tlm@petrochina.com.cn (Z. Xu), zhoulu-tlm@petrochina.com.cn (L. Zhou), housy-tlm@petrochina.com.cn (S. Hou).

https://doi.org/10.1016/j.marpetgeo.2023.106528
Received 9 April 2023; Received in revised form 25 September 2023; Accepted 26 September 2023
Available online 27 September 2023

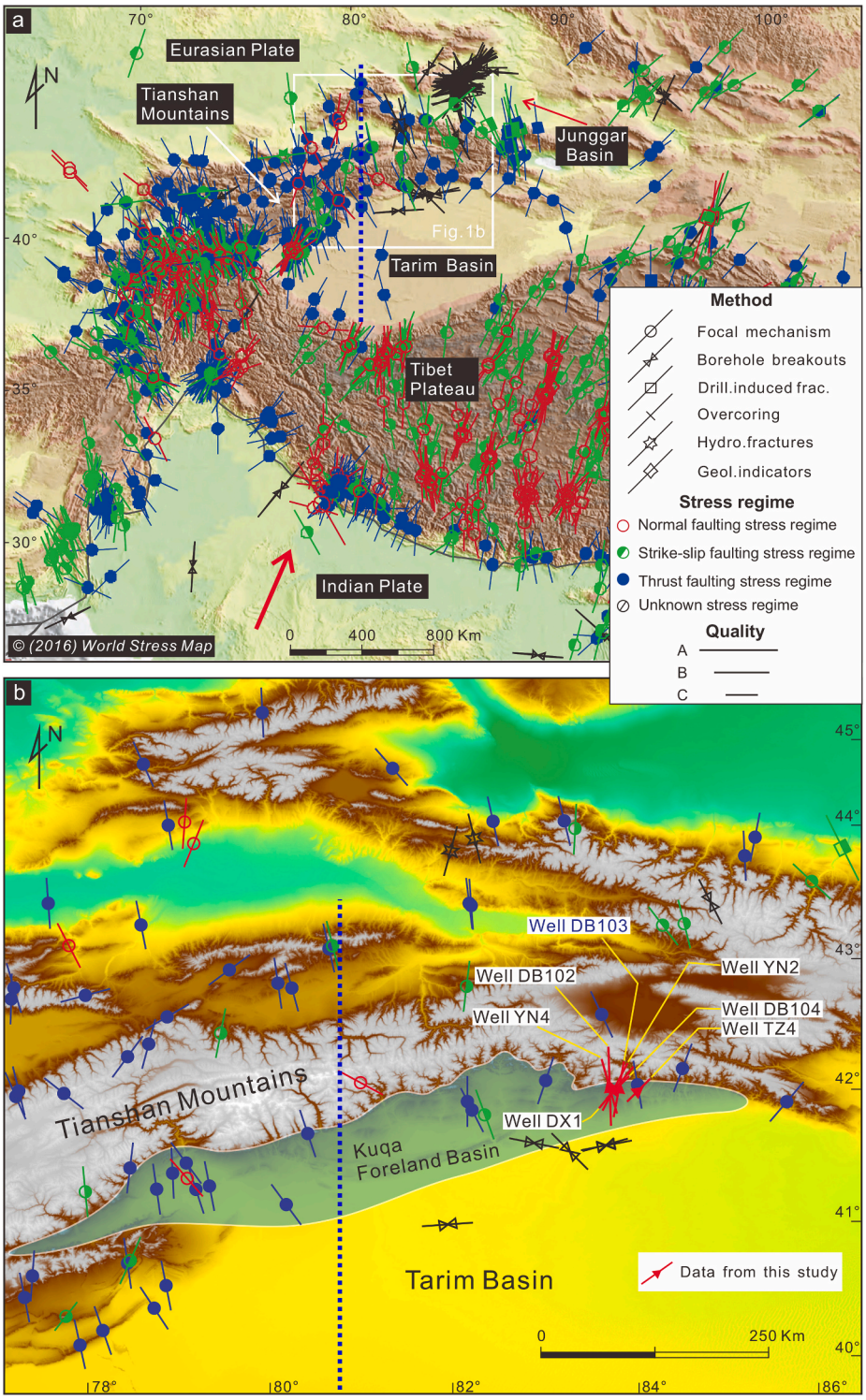

Fig. 1. (a) Maximum horizontal stress (S_{Hmax}) orientations in the Tarim Basin and adjacent regions from the World Stress Map (WSM) database (Heidbach et al., 2016). The bars denote S_{Hmax} orientations with lengths being proportional to data quality; symbols represent the method of stress measurement. The thick red arrow indicates the motion direction of the Indian Plate relative to the Eurasian Plate; (b) S_{Hmax} orientations from WSM and this study are plotted on the topographic map of the Tianshan Mountains generated from data fusion of Shuttle Radar Topography Mission 15 (SRTM 15) for comparison. The dotted bold blue line marks the regional S_{Hmax} orientation in northwestern China (Hu et al., 2017).

Heidbach et al., 2010; Hu et al., 2017).

Against the background of the first-order stress pattern, local stress pattern (second to third-order stress) (<500 km) can be perturbed frequently. Fault is well documented as one of the important geological factors deviating local stress field from the first-order stress field and generate new stress patterns in sedimentary basins (Barton and Zoback, 1994; Yale, 2003; Tingay et al., 2010; Gudmundsson et al., 2010; Rajabi et al., 2016a and b; Radwan et al., 2021; Wang et al., 2022); the fault-induced stress orientation is due to slippage along preexisting faults or faulting-related elastic heterogeneity (Shamir and Zoback, 1992; Gudmundsson et al., 2010; Tingay et al., 2010). Moreover, fracturing has been recognized as another important geological factor

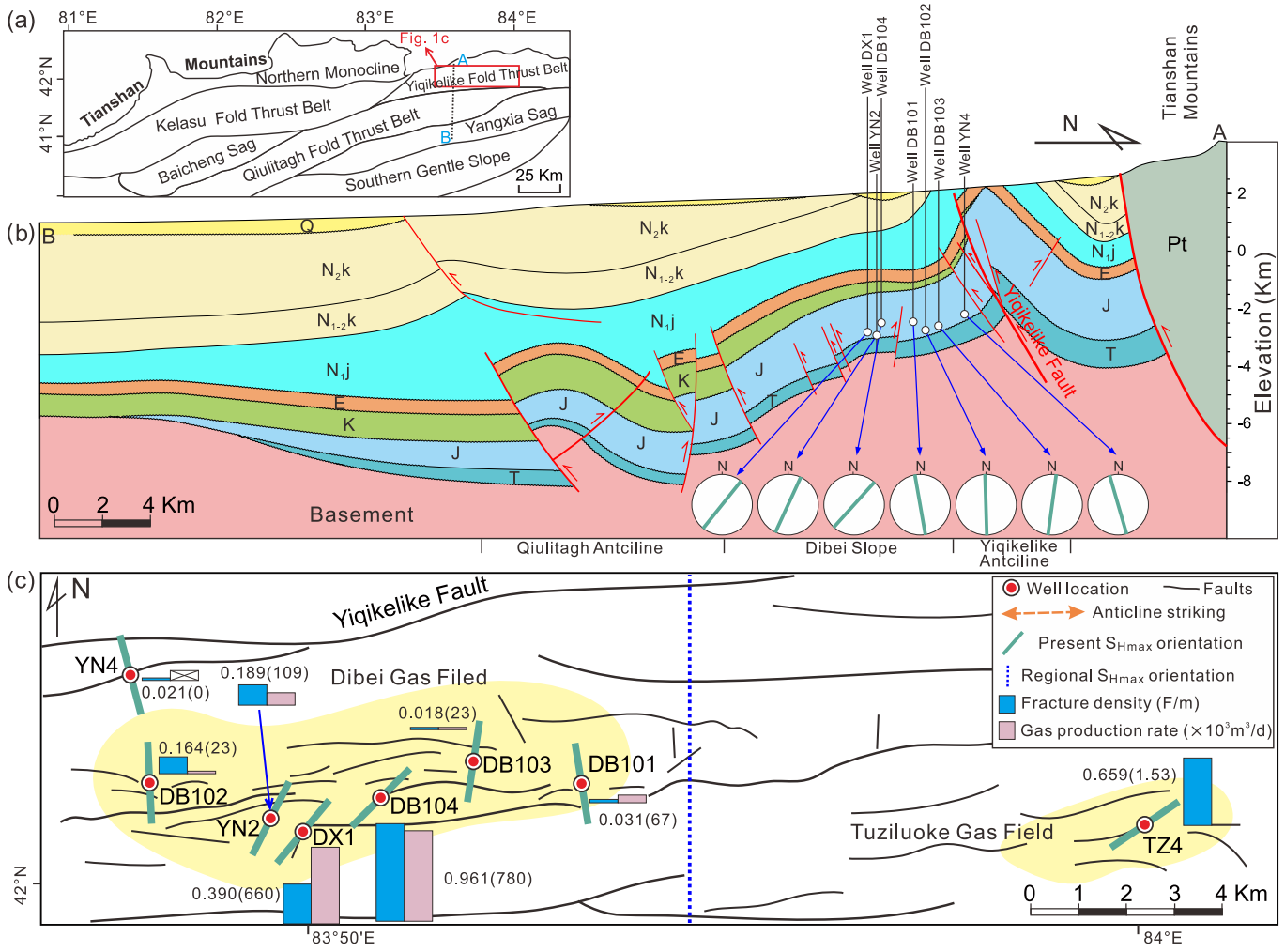

Fig. 2. Structural map and cross section and S_{Hmax} orientations in the study area. (a) Map showing the major structural units in the Kuqa Foreland Basin; (b) An interpreted seismic line across the study area showing faults, fault-related folds and projection of analyzed wells onto the line with S_{Hmax} orientations (note that well TZ4 is not included in the profile). See Fig. 2a for the line location; (c) S_{Hmax} orientations, fracture densities and gas production rates were plotted on the structural map of uppermost Ahe Formation. The dotted blue line represents the regional S_{Hmax} orientation in northwestern China (Hu et al., 2017). Numbers next to bars denote fracture densities (F/m) with gas production rate ($\times 10^3$ m^3/d) in brackets.

leading to more local stress deflection or rotation (Faulkner et al., 2006; Heap et al., 2010; Lin et al., 2010; Rajabi et al., 2016a and b). Numerical simulation results have revealed that rock heterogeneity related to fracturing and diagenesis accounts for local stress reorientation (Zhang et al., 1994). Similarly, Local S_{Hmax} orientation perturbation has been interpreted to be caused by juxtaposition of stiff and soft materials (Bell, 1996).

The World Stress Map (WSM) database shows that plate boundary forces generated from the collision between Eurasian and Indian plates exert first-order controls of the stress pattern with S_{Hmax} in a N–S direction in northwestern China (Fig. 1a) (Hu et al., 2017). Collision between the two plates was also considered to account for the Neogene uplift of the Tianshan Mountains (Molnar and Tapponnier, 1975; Tapponnier and Molnar, 1979; Lu et al., 2000), an East-West (E-W) trending range lying between the Tarim and Junggar basins in northwestern China (Fig. 1a). Previous studies have noted the variation in S_{Hmax} orientation in the Kuqa Foreland Basin adjacent to the Tianshan Mountains (Zhang and Wang, 2004; Nian et al., 2016; Zhang et al., 2020). Recently, Wang et al. (2022) observed appreciable stress rotation in the vicinity of faults in the western Kuqa Foreland Basin. Nevertheless, little attention was paid to the geological factors resulting in the stress variation.

In this study, we investigated *in-situ* stress orientations and subsurface fractures in the Jurassic sections with burial depths in excess of 4000 m from the Dibei-Tuziluoke Gas field, Kuqa Foreland Basin. *In-situ* S_{Hmax} orientations were determined by borehole breakouts and drilling-induced fractures interpreted from borehole images. S_{Hmax} orientations in this study were compared with those derived from the earthquake focal mechanism solutions in the Tianshan Mountains from the WSM to ascertain whether S_{Hmax} orientations are controlled by plate boundary forces. We analyzed lateral (between wells) and depth-dependent (within a well) variation in stress orientations to investigate factors that account for the local variation in stress orientations. We then analyzed the relationship between fracturing and stress orientation.

2. Geologic setting

The Kuqa Foreland Basin lies to the south of the Tianshan Mountains, and is a sub-basin located in the northern Tarim Basin in northwestern China (Fig. 1). The Kuqa Foreland Basin can be divided tectonically into the Northern Monocline, Yiqikelike-Kelasu Fold Thrust Belt, Baicheng Sag, Qiulitagh Fold Thrust Belt, Yangxia Sag and Southern Gentle Sag (Fig. 2a). The basement under the foreland basin comprises Paleozoic igneous rocks and the basin has been filled by an extremely thick (>10 km) Mesozoic and Cenozoic sedimentary sequence, from the Triassic

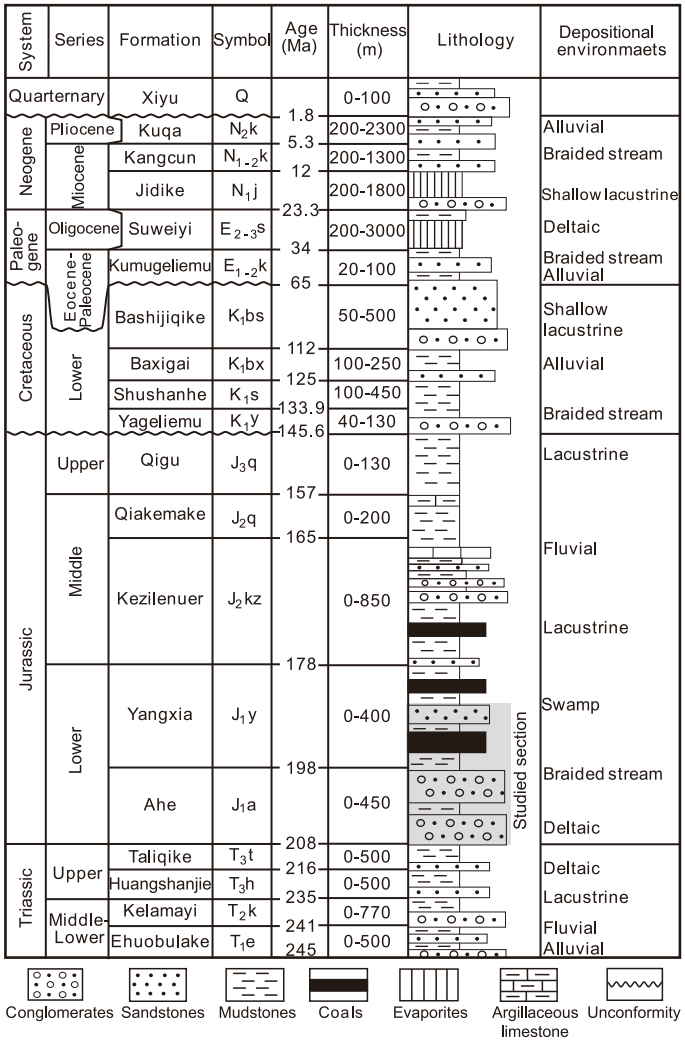

Fig. 3. Composite stratigraphic column showing formations stratum thickness, lithology, and depositional environments in the Kuqa Foreland Basin (stratigraphic column modified after Liu et al., 2016; depositional environments after Zhu et al., 2009).

Table 1
Image logs used in this study. J_1a = Ahe Formation; J_1y = Yangxia Formation.

Image logs	Wells	Depth interval (m)	Formation
FMI	DB101	4785–5099	J_1a
	DB102	4930–5222	J_1a
	DB104	4690–4770	J_1y, J_1a
	DX1	4885–5005	J_1a
FMS	YN2	4489–4628, 4679–4779	J_1y, J_1a
	YN4	4093–4700	J_1y, J_1a
XRMI	TZ4	4172–4310	J_1a
	DB103	4612–4723	J_1y, J_1a

through to the Quaternary, that was primarily deposited in fluvial and deltaic environments (Zhu et al., 2009) (Fig. 3). These sedimentary sequences have been involved in a thrust system that propagated southwards from the Tianshan Mountains to the basin since the Neogene (Fig. 2b). The deformation is dominated by a series of north-dipping imbricated faults and fault-related folds (Qiulitagh Anticline and Yiqikelike Anticline), and more pliable rocks such as Jurassic coals and Paleogene and Neogene evaporites play an important role in regulating deformation (He et al., 2009) (Fig. 2b).

The Late Paleozoic Era (from the Late Carboniferous to the Early Permian) witnessed the agglomeration of multiple continental blocks, development of the Paleozoic Tianshan Orogeny and the change from marine into terrestrial environments in the Kuqa area (Charvet et al., 2011; Xiao et al., 2013; Alexeiev et al., 2015). From the Late Triassic to the Middle Jurassic, the paleo-climate was warm and humid. The Kuqa Foreland Basin was filled by deltaic and lacustrine sediment in terrestrial environment. The two main source rocks for the basin, oil prone Triassic mudstones and gas prone Jurassic coals, were developed under a deep lacustrine and swamp setting respectively during this period (Hendrix, 1992; Li et al., 2000, 2004).

During most of the Mesozoic and even into the Paleogene, Tianshan Orogeny and Kuqa region were tectonically tranquil and dominated by extensive planation (Li et al., 2004; Jia, 2013; Jolivet et al., 2013; Morin et al., 2019). Marine flooding from the western Tarim Basin and its retreat during the Cretaceous to the Paleogene were responsible for the deposition of the thick Paleogene and Neogene evaporites (Guo et al., 2002; Liu et al., 2013; Li et al., 2017), which provide a regional seal for petroleum accumulation. During the earliest Paleogene Period (*ca.* 59 Ma), the Indian Plate collided with the Eurasian Plate (Hu et al., 2015), initiating an active tectonic cycle. In response to the collision and the uplift of the Tianshan Mountains, the Kuqa Foreland Basin experienced increasingly intense tectonic shortening from 36 Ma onwards, with a shortening rate reaching its peak during the Pliocene (Zhang et al., 2014).

The study area covers Dibei Gas Field (wells YN4, DB102, YN2, DX1,

Table 2
Quality ranking for S_{Hmax} orientations inferred from drilling-induced failures (after Heidbach et al., 2010). BOs = Borehole breakouts; DIFs = Drilling-induced fractures; QR = Quality ranking.

Stress indicator	Well	Latitude	Longitude	Count	Combined Length (m)	S.D.(deg)	Mean orientation (deg)	S_{Hmax} Azimuth (deg)	QR
BOs	DB103	42°08′07.00″	83°52′13.99″	19	46	8.8	98.59	188.59	B
	DB104	42°07′42.97″	83°50′41.19″	6	20.5	24.6	135.12	45.12	C
	TZ4	42°06′55.7″	84°03′11.4″	71	45.54	26.85	147.77	57.77	D
	DB102	42°08′03.13″	83°46′55.54″	41	116.25	7.96	87.28	177.28	A
	DX1	42°07′21″	83°49′22″	42	75.7	14.8	127.96	37.96	B
	DB101	42°07′51.72″	83°54′0.11″	6	6.9	24.14	80.79	170.79	D
	YN2	42°07′32″	83°48′50″	25	96.45	13.85	116.65	26.65	B
	YN4	42°09′19″	83°46′41″	56	148.7	15.21	75.08	165.08	B
DIFs	TZ4	42°06′55.7″	84°03′11.4″	23	37.8	14.38	63.53	63.53	C
	DX1	42°07′21″	83°49′22″	2	8.9	2.82	33.00	33.00	D

DB104, DB103 and DB101) in the south-dipping Dibei Slope between the Qiulitagh and Yiqikelike Anticlines and Tuziluoke Gas Field (Well TZ4) (Fig. 2b and c). E-W trending reverse faults are well developed across the study area (Fig. 2c). The Jurassic Ahe Formation sandstones constitute major reservoirs for the gas field, which are generally tight with a porosity ranging from 2.6 to 9.5% and a permeability between 0.02 and 2.0 × mD (Wang et al., 2020). High permeability (>1 mD) is usually due to the presence of fractures. Fracture development is considered to be primarily controlled by faults, lithology and structural positions (Ju et al., 2013, 2018; Zhan et al., 2014). It has been proposed that fractures have formed since the Paleogene, with the S_{Hmax} orientation assumed to be constantly in the N–S direction (Jiang et al., 2015). Fractures are not only important for petroleum migration and accumulation and formation of sweet spots (Lu et al., 2016), but also enhance petroleum production significantly (Ju and Wang, 2018).

3. Materials and methods

3.1. Materials and database

Borehole image logs used in this study including Schlumberger's Formation Microscanner (FMS) and Fullbore Formation Microimager (FMI) and Halliburton's ten (XRMI). Table 1 details the information about borehole image logs used in this study in terms of wells, depths and formations. Processing of image logs was performed before interpretation using Schlumberger's software *Techlog,* and a standard workflow was followed including imaging speed correction, eccentering correction and image normalization (Lai et al., 2018). Baker Hughes's XMAC™ (Cross Multipole Array Acoustilog) logs were available for wells DB102, 103 and TZ4 and Schlumberger's DSI™ (Dipole Shear Sonic Imager) logs were available for wells DB101, DB104 and DX1. Neither XMAC nor DSI logs were measured for wells YN2 and YN4.

Lithology data obtained from drilling cutting analysis were available for wells DB103, YN2 and TZ4 and depths of the lithology data were calibrated to exactly correspond with the depths of image and conventional logs (gamma ray) by identifying and correlating distinctive features (mudstone layers). Porosity data from logs were available for wells DX1 and TZ4. Hydrostatic and formation pressures were estimated respectively for well TZ4 using formation water and drilling mud densities respectively; the formation water density was determined on water samples using the scaling method. Formation pressure can be estimated from drilling mud density because bottom hole pressure is controlled by adjusting mud weight to be close to the expected pore pressure during drilling (Beaumont and Foster, 1999). The formation pressure coefficient was calculated using the ratio of formation to hydrostatic pressure. All data were provided by the Institute of Petroleum Exploration and Development, Tarim Oil Field Company.

3.2. Fracture analysis

The picking of natural fractures and bedding planes was made manually. On borehole images, natural fractures were recognized by dark or bright and continuous or discontinuous sinusoidal wave appearances depending on conductivity of borehole fluids and cement degree of fractures, respectively (Khoshbakht et al., 2009; Rajabi et al., 2010; Lai et al., 2018). Image logs operated in wells that were drilled with water-based drilling muds can reflect whether fractures are electrically conductive or not, and electrically conductive fractures are conventionally assumed to be open (Lai et al., 2018). Bedding planes can also appear as sinusoidal on borehole images. However, they occur as interfaces between lithological units that show distinct colors on borehole images owing to contrast in conductivity and thus can be easily distinguished from natural fractures.

The poles to planes of fractures interpreted from borehole images were plotted in stereograms (Schmidt lower hemisphere) using the software Stereonet v.11.3.5 (released by Allmendinger R.W. from Cornell University, USA). Densities of fracture populations were plotted as contour lines in the background of the stereograms using Kamb distribution as contouring method. Bedding planes recognized from borehole images were not rotated back to horizontal. Since all the wells included in the present study were vertical, dip correction was thus not required.

Fracture densities are usually used to assess fracture development; the usage of fracture densities, however, varies, and depends highly on the measuring dimensions (1D, 2D or 3D) (Lorenz and Cooper, 2020). Here fracture density is defined as the number of natural fractures per unit length along the borehole (1D). For the purpose of assessing fracture development between wells or at different depth intervals within a well, fracture density was calculated using the following equation:

$$D = N/L \quad (1)$$

where D is fracture density, N is the number of fractures within an analyzed borehole interval with a length of L (m). Fractures were also counted every meter along the borehole of a well to obtain a continuous fracture density logs.

3.3. In-situ stress orientation analysis

In-situ stress orientations can be determined using borehole breakouts and drilling-induced fractures, which occur as diagnostic appearances on borehole images. Borehole breakouts and drilling-induced fractures can thus be differentiated from each other distinctly.

Borehole breakouts (BOs) are stress-induced wellbore enlargements (Bell and Gough, 1979). BOs occur because of failure of borehole wall when stress concentrations at the borehole exceed the rock strength (Zoback et al., 1985; Tingay et al., 2008). BOs occur perpendicular to the direction of the maximum horizontal stress (S_{Hmax}) and are recognized as pairs of vertical bands that are generally parallel to borehole axis and separated by approximately 180° on borehole images (Tingay et al., 2008; Rajabi et al., 2010, 2016a; Lai et al., 2018). It should be noted that breakout color on borehole images is dependent on the conductivity of borehole fluids; when the borehole is filled with water-based drilling

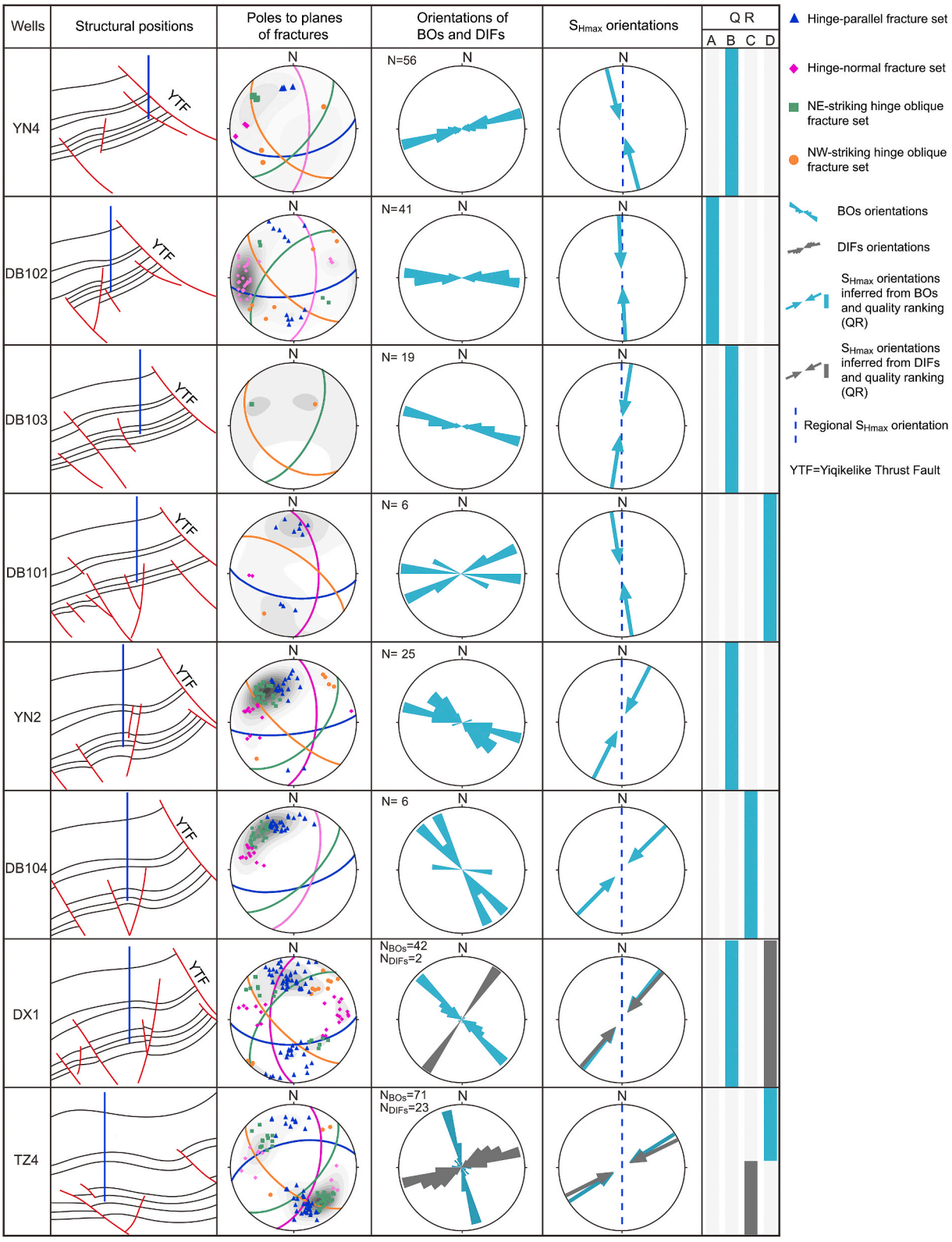

Fig. 4. Composite diagram showing structural positions and orientations for natural fractures, borehole breakouts and drilling-induced fractures as well as S_{Hmax} orientations for the analyzed wells. Structural positions are interpreted from seismic profiles, with solid blue lines in the structural position column representing well trajectories. Stereograms show poles to planes of natural fractures; symbols represent different fracture sets, and lines denote the mean orientation for corresponding fracture sets; densities of fractures are shown by monochrome-filled contour lines in the background. *In-situ* S_{Hmax} orientations are derived from borehole breakouts (BOs) and drilling-induced fractures (DIFs), and their quality ranking (QR) is evaluated using the scheme proposed by Heidbach et al. (2010).

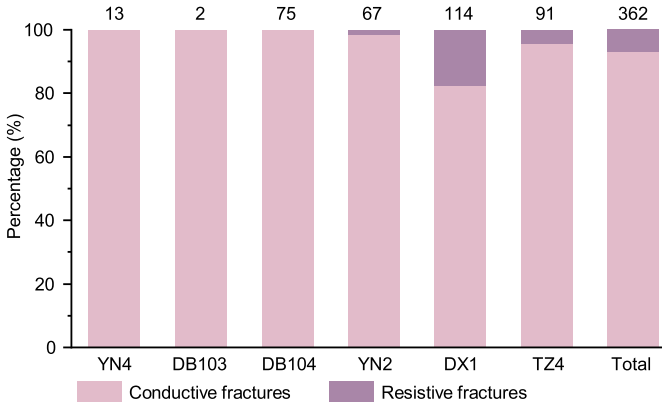

Fig. 5. Percentage of conductive and resistive fractures in the study area. Note that only fracture data from wells drilled with water-based drilling muds was used. Numbers at bar top denote fracture numbers analyzed.

fluid, the breakouts appear as dark bands, while bright breakouts occur when the drilling fluid is of oil-based (Nian et al., 2016). In this study, wells DB101 and 102 were drilled with oil-based drilling muds, while the other wells were drilled with water-based drilling muds.

Drilling-induced fractures (DIFs) are recognized as pairs of narrow fractures that are parallel to borehole axis but separated by approximately 180° on borehole images (Brudy and Zoback, 1999; Nian et al., 2016; Rajabi et al., 2016a; Lai et al., 2018). DIFs develop when the circumferential stress exceeds the tensile strength of the borehole wall and are thus oriented roughly parallel to the *in-situ* S_{Hmax} orientation (Aadnoy and Bell, 1998; Tingay et al., 2008).

In-situ S_{Hmax} orientations for each well were determined using the average azimuth of BOs and DIFs observed in this study. S_{Hmax} orientation results were then assigned a quality ranking according to a scheme that is based on the standard deviation, number, and total length of DIFs and BOs (Heidbach et al., 2010). The scheme defines a quality ranking ranging from A-quality (most reliable, S_{Hmax} within ±15°) through to E-quality (with no reliable information). S_{Hmax} orientations with A to C quality are commonly believed to be reliable. These S_{Hmax} orientation results were then used to reveal the lateral variation in S_{Hmax} orientation between wells. Depth-dependent variations in the S_{Hmax} orientation were investigated using three wells DB103, YN2 and TZ4; these wells were chosen since they are located in different structural locations and have distinct fracture development and S_{Hmax} orientations.

3.4. Computation of dynamic Poisson's ratio

In order to investigate the impact of fracturing on the elastic parameters, XMAC and DSI logs were used to compute the dynamic poisson's ratio in this study. PetroChina's software CIFlog™ was used to

Table 3
Density of different fracture sets and aggregate fractures in the study area (unit: F/m). Hpa = Hinge-parallel fractures; Hn = Hinge-normal fractures; HONE = NE-striking hinge-oblique fractures; HONW = NW-striking hinge-oblique fractures; J1y = Yangxia Formation; J1a = Ahe Formation.

Wells	YN4	DB102	DB103	DB101	DB104	YN2	DX1	TZ4	Remarks
Depthinterval (m)	4093–4700	4930–5222	4612–4723	4785–5099	4690–4770	4489–4628, 4679–4779	4885–5005	4172–4310	
Formation	J_1y, J_1a	J_1a	J_1y, J_1a	J_1a	J_1y, J_1a	J_1y, J_1a	J_1a	J_1a	
Hpa	0.00494	0.03647	0	0.02353	0.33766	0.06834	0.21254	0.2971	Formed as a result of stress partition during fold development.
Hn	0.00494	0.09422	0	0.00471	0.16883	0.03467	0.08014	0.08696	Formed during the post-folding stage (Yu et al., 2016).
HONE	0.00659	0.01216	0.00901	0.00235	0.45455	0.07334	0.05226	0.25362	HONW and equivalent HONE formed as conjugated fracture sets under the regional stress field during the pre-folding stage. Stress re-orientation during post-folding stage is another cause for HONE development.
HONW	0.00494	0.02128	0.00901	0	0	0.0125	0.0453	0.02174	
Aggregate	0.02142	0.16413	0.01802	0.03059	0.96104	0.18885	0.39024	0.65942	

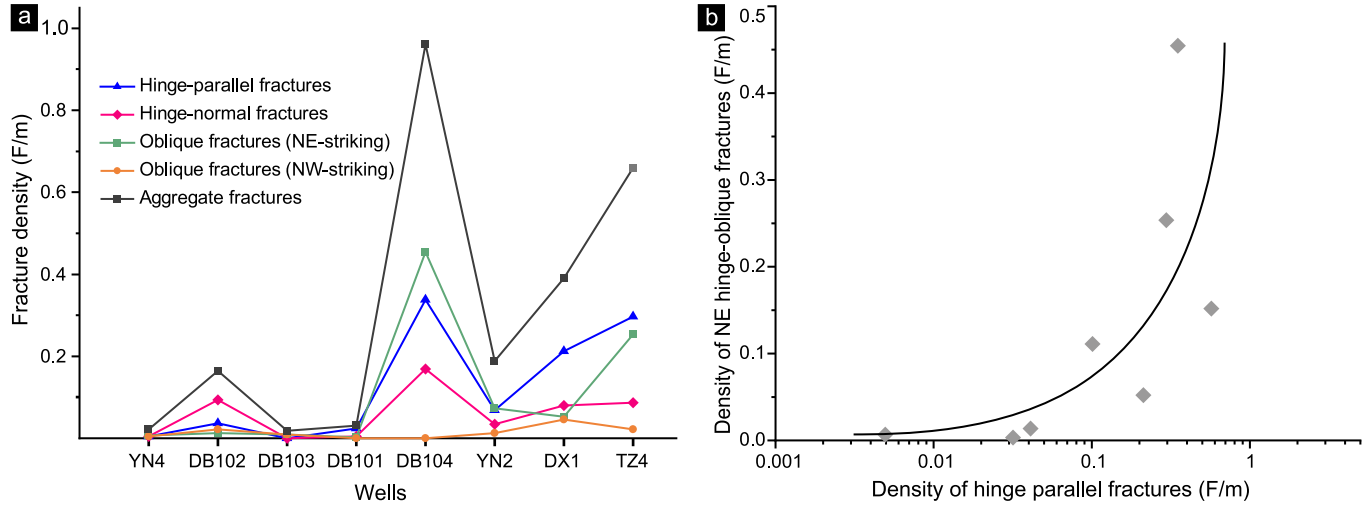

Fig. 6. (a) A plot showing densities of different fracture sets and aggregate fractures; (b) A plot showing the positive correlation between densities of hinge-parallel fractures and NE-striking hinge-oblique fractures.

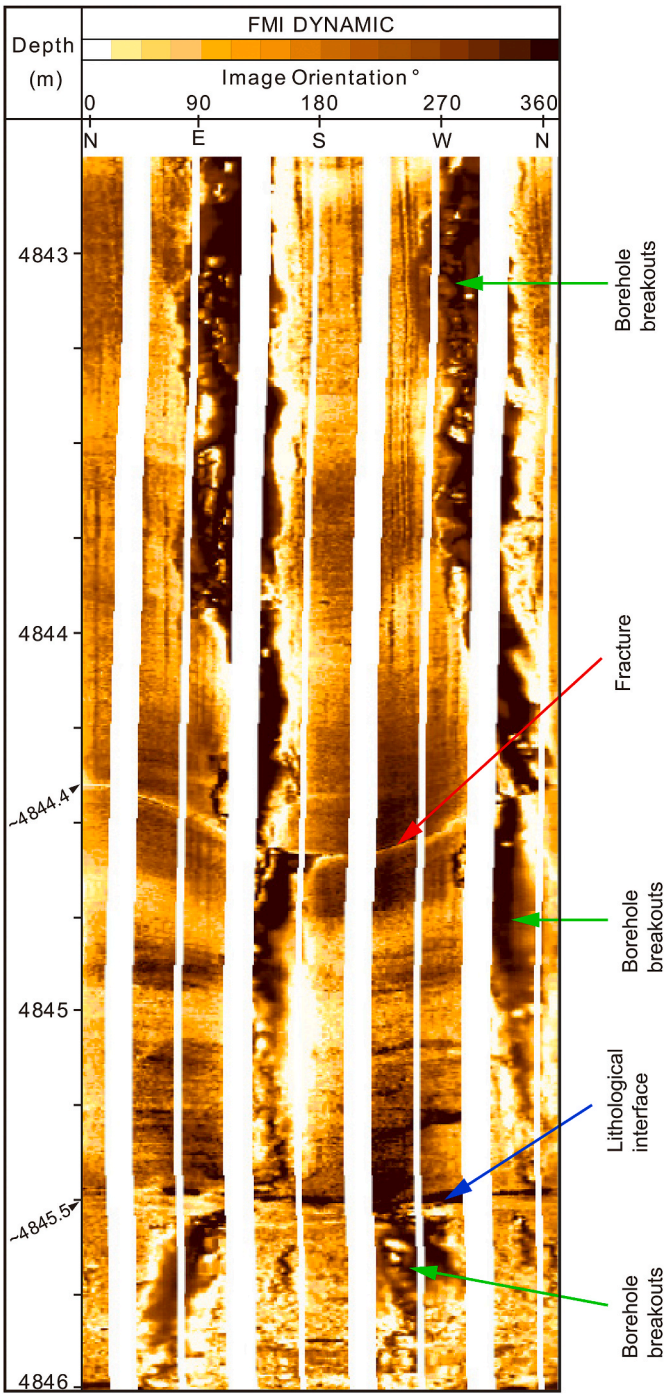

Fig. 7. Borehole image from well DX1 showing rotation of borehole breakouts (green arrows) in the vicinity of a fracture (red arrow) and lithological interface (blue arrow).

process the raw XMAC and DSI data to extract shear and compressional sonic slowness data. Data were processed according to processing procedure in the software CIFlog™, including data decompilation, sonic slowness extraction, borehole compensation, sonic slowness correction. Shear sonic slowness exacted for Well DB103 display a poor data quality because of significant signal attenuation, which is probably related to the presence of extensively coal seams in this well. The sonic slowness data for the well were thus not computed. Dynamic elastic variables (Poisson's ratio) for the other five wells (DB102, DB101, DB104, DX1 and TZ4) were computed by using extracted sonic slowness data via the following equations:

$$\mu_d = \frac{2 - DTS^2/DTC^2}{2\left(1 - DTS^2/DTC^2\right)} \quad (2)$$

where μ_d is the dynamic Poisson's ratio, DTS and DTC are shear and compressional sonic slowness in μs/ft, respectively.

4. Results

4.1. Lateral variation in S_{Hmax} orientation

Both borehole images and array sonic logs are reliable indicators of the *in-situ* S_{Hmax} orientations (Lai et al., 2022). In this study, a total of 266 borehole breakouts and 25 drilling-induced fractures recognized from borehole images were used to determine *in-situ* S_{Hmax} orientations. Borehole breakouts were observed in all eight wells, while drilling-induced fractures were only developed in well TZ4 and DX1. S_{Hmax} orientations derived from breakouts are generally ranked as A- to C-quality except two wells (wells DB101 and TZ4) that are ranked as D-quality (Table 2). The S_{Hmax} orientation derived from drilling-induced fractures is ranked as C-quality for well TZ4 and D-quality for well DX1. S_{Hmax} orientations in this study vary markedly on a scale of less than 10 km and seem to occur as two distinctly different stress patterns. The first stress pattern including data from wells YN4, DB102, DB103 and DB101, all located in a south-dipping panel between two faults, has stress orientations between NNW to NNE (165–188.59 °N) (Fig. 1b, 2c and 4). In contrast, S_{Hmax} orientations for the second stress pattern (wells DB104, DX1, TZ4 and YN2) range from NNE to ENE (26.65–63.53 °N). These wells are situated in a weakly developed anticline influenced by faults (Fig. 1b, 2b and 4).

Smoothed results of S_{Hmax} orientations derived from multiple stress indicators (earthquake faulting mechanisms, borehole breakout and drilling-induced fractures et al.) on a continental scale suggest that S_{Hmax} orientation in northwestern China is in north-south direction (Fig. 1a). The collision between the Eurasian and Indian plates is considered to have the first-order (>500 km) control on the regional stress pattern (Hu et al., 2017). This knowledge about continental scale stress pattern provides a foundation for us to determine the stress sources and identify the perturbation of local stress field. It has been proposed that the S_{Hmax} orientations in the Kuqa Foreland Basin are generally in north-south and controlled regionally by the collision between the Eurasian and Indian plates (Jia, 2004; Zeng et al., 2010). The interpretation appears to be compatible with ENE to EW trending thrust faults and fault-related folds in the Kuqa Foreland Basin adjacent to the Tianshan Mountains (Fig. 2a and c). However, results presented here indicate that the sources of stress pattern in the Kuqa Foreland Basin are more complicated than previously thought.

First stress pattern in the study area is approximately consistent with the regional stress field (N–S direction) in northwestern China (Fig. 1b, 2c and 4). We therefore interpreted that the first stress pattern has a regional or first-order origin (>500 km) and is controlled by plate boundary forces related to the Eurasian-Indian plate collision. The S_{Hmax} orientations of the second stress pattern are clearly incompatible with the first-order or regional stress pattern (Fig. 1b, 2c and 4). Plate collision thus cannot provide a rational explanation for the stress pattern observed in these wells. On the contrary, it indicates that S_{Hmax} orientations manifested in these wells have been perturbed or rotated. Faults appear to have changed S_{Hmax} orientations, since wells immediately adjacent to faults typically display deviations in stress orientations from the north-south regional trend albeit to varying extents, for example in wells DB104, DX1 and TZ4 (Fig. 2c). The recently identified local stress reorientation related to faulting in the Kuqa Foreland Basin further attested our interpretation (Wang et al., 2022).

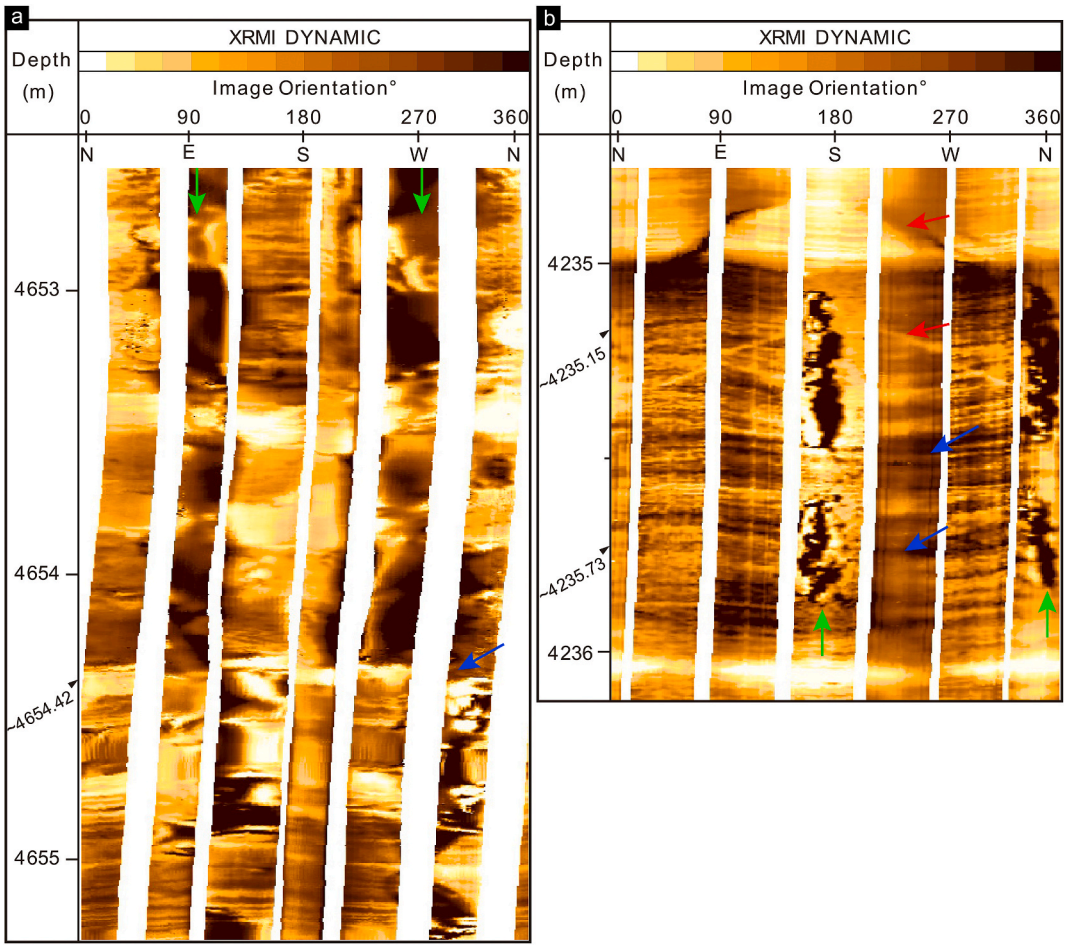

Fig. 8. Borehole images showing rotation of borehole breakout (green arrows) in the vicinity of fractures (red arrows) and lithological interfaces (blue arrows). Example from (a) well DB103; (b) well TZ4.

4.2. Fracture analysis

Fracture data from wells drilled with water-based drilling muds (wells YN4, DB103, DB104, YN2, DX1 and TZ4) suggests that *ca.* 96% natural fractures are conductive fractures (Fig. 5), which are probably open or not completely filled by minerals. Natural fractures were categorized on the basis of fracture orientations relative to fold striking in this study: (1) hinge-parallel fractures, (2) hinge-normal fractures, (3) NE-striking hinge-oblique fractures and (4) NW-striking hinge-oblique fractures (Fig. 4). Hinge-parallel fractures and NE-striking hinge-oblique are dominant fracture sets in the study area and both sets show highly variable densities between wells (Fig. 4). Hinge-normal fractures are less dominant and NW-striking hinge-oblique fractures are poorly developed across the study area.

The density of different fracture sets and aggregate fractures are presented in Table 3 and Fig. 6a. Results indicate that fractures are well developed in wells DB104 and TZ4, and aggregate fracture densities in the two wells are 0.961 and 0.66 F/m, respectively. Hinge-parallel and NE-striking hinge-oblique facture densities in well DB104 are 0.34 and 0.45 F/m, respectively; the two fracture sets in well TZ4 have densities of 0.30 and 0.25 F/m, respectively. wells DX1, YN2 and DB 102 have moderate densities of aggregate fractures with density values of 0.39, 0.19 and 0.16 F/m, respectively and wells YN4, DB101 and DB103 have aggregate fracture densities less than 0.03 F/m. Fractures are sparsely distributed in these wells and only two fractures were observed in well DB103. A moderately positive correlation exists between the density of hinge-parallel and NE striking hinge-oblique fractures (Fig. 6b).

Previous studies proposed that subsurface fractures in the study area formed in three phases since the onset of the Paleogene and hypothesized that the S_{Hmax} orientation was in the N–S direction and remained unchanged during fracture formation (Jiang et al., 2015). Our observation, however, shows that the S_{Hmax} orientations in the study area have been perturbed or rotated by local geological factors. The development of hinge-parallel fractures and NE-striking oblique fractures seems to be controlled by structural positions: wells located near the crest of gentle fault-related anticlines, for example, wells DB104 and TZ4, typically display the highest densities of hinge-parallel fractures and NE-striking oblique fractures of all the wells studied (Figs. 4 and 6a). These fractures appear unlikely to form prior to fold development but are probably related to the deformation associated with the development of the Yiqikelike Anticline. Hinge-parallel fractures were considered to form as a result of stress partition owing to the presence of finite and incremental neutral planes during the development of fault-related fold in the Kuqa Foreland Basin (Sun et al., 2017). The fracture set is thus interpreted to have developed during the syn-folding stage before stress reorientation in the context of a S_{Hmax} orientation consistent with regional stress field.

NE-striking oblique fractures are parallel or sub-parallel to the present-day S_{Hmax} orientations (Fig. 4), suggesting these fractures formed recently (Rajabi et al., 2010; Ameen, 2016). Most NE-striking oblique fractures are interpreted here to be the youngest fracture set formed during the post-folding stage. NW-striking hinge oblique fractures are poorly developed across the study area, and their densities show no marked variations between wells (Fig. 6a). These fractures, and equivalent NE-striking hinge-oblique fractures, are considered to have formed as conjugated fracture sets under the regional stress field during

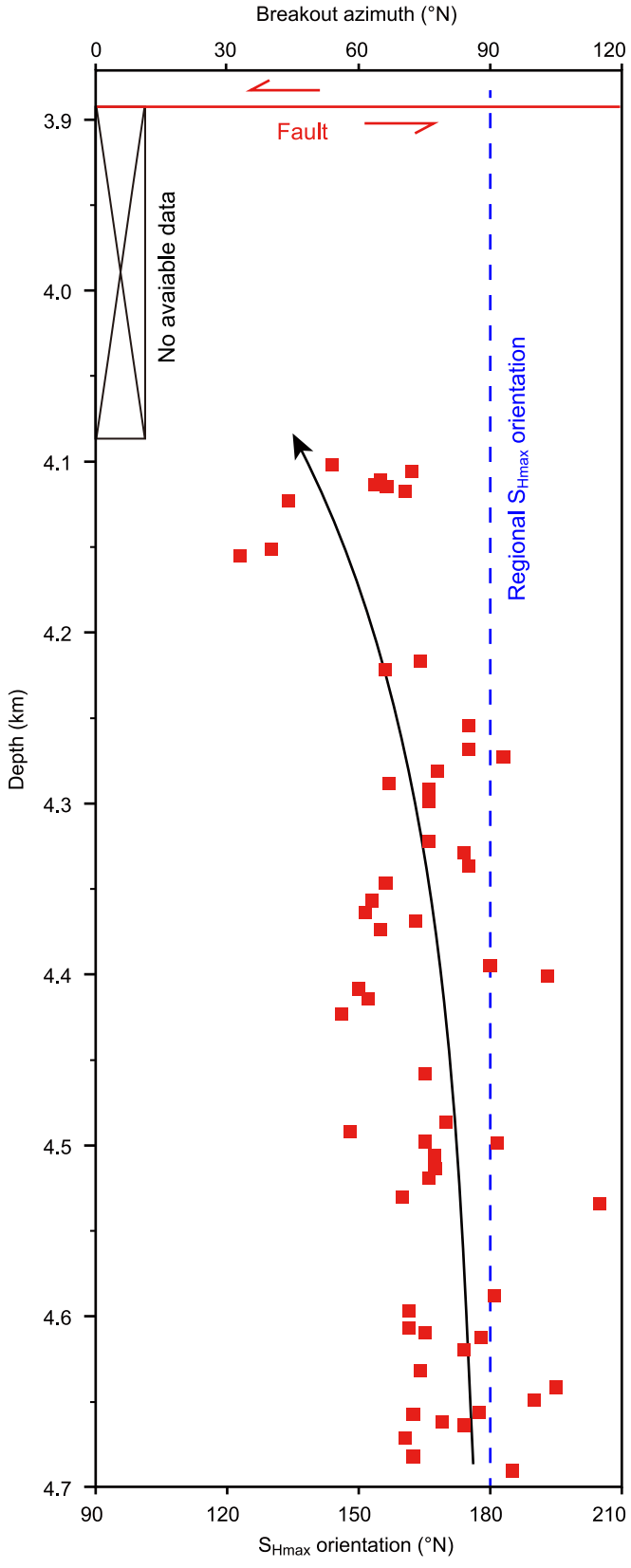

Fig. 9. Depth-dependent S_{Hmax} orientations derived from borehole breakouts for well YN4 showing gradual deviation of stress orientations from the regional trend as the fault is approached. Note that stress and breakout orientations are plotted in one track by using the same symbol but different azimuth coordinates.

the pre-folding stage (Jiang et al., 2015). Hinge-normal fractures were proposed to have formed during the post-folding stage (Yu et al., 2016).

4.3. Depth-dependent variations in the orientation of S_{Hmax}

Breakout orientations usually show rotation in the vicinity of fractures and lithological interfaces (Fig. 7 and 8). For example, breakouts have rotated across the fracture at a depth of ~4844.4 m and the lithological interface at ~4845.5 m for well DX1 (Fig. 7). Another good example illustrating breakout rotation related to lithological interface is at ~4654.42 m in well DB103 (Fig. 8a). In some cases, breakout rotation caused by fractures and lithological interfaces may be less evident, for instance the fracture at ~4235.15 m and the lithological interface at the depth of ~4235.73 m (Fig. 8b). All these fluctuations of breakout azimuths actually reflect vertical variations in S_{Hmax} orientations.

No recognizable faults on seismic profile intersect vertically with the studied intervals for all wells (Fig. 4). However, there is an example from well YN4 where depth-dependent stress orientations deviate from the regional trend as the fault is approached (Fig. 9), reflecting the active role of the fault in changing stress orientation.

Continuous S_{Hmax} orientation profiles were obtained based on breakout azimuths for three representative wells to analyze depth-dependent variation in S_{Hmax} orientations. These profiles have been divided into discrete units based on discrepancy in fracture development and S_{Hmax} orientation variations. The rotation of S_{Hmax} orientations in well DB103 (only two fractures were identified in the well) is relatively minor in most cases with degrees less than 10 (units A and C in Fig. 10), and rotation usually occurs in the vicinity of lithological interfaces. A marked change in S_{Hmax} orientation up to 20° occurs at the interface between units A and B, where porosity vary abruptly. The overall S_{Hmax} orientations in the well are close to the regional stress direction (Fig. 10). Well YN2 is more fractured with more variable stress orientations (standard deviation = 13.85) (Table 2). Variations in S_{Hmax} orientations in poorly fractured units are usually slight and no more than 10°; these variations are typically related to lithological changes and show slight to moderate deviation from the regional trend (Unit D in Fig. 11). S_{Hmax} orientations in well-fractured units in the well, however, vary markedly (variations ranging from 5 to 45°) and overall S_{Hmax} orientation trend in these units usually deviate significantly from the regional trend with maximum deviation up to 50° (Units F and G in Fig. 11).

Breakouts with highly variable orientations are well developed in well TZ4 (Fig. 12), which produced an unreliable and a low quality ("D") rank for the determination of S_{Hmax} orientations. Nonetheless, the well provides a good opportunity for further investigating the relationship between the depth-dependent S_{Hmax} orientation and fracture development. It is evident that significant rotation (23.6–55°) of the S_{Hmax} orientation normally occurs in the vicinity of interfaces between well-fractured units and fracture-free units (Fig. 12), for example, the interfaces between ML2 and ML3, ML3 and ML4 and ML5 and ML6. S_{Hmax} orientations in well-fractured units usually deviate from regional trend (Units ML1, ML2, ML4 and ML5) with deviations ranging from 50–77°, while S_{Hmax} orientations for fracture-free units (ML3 and ML6) are relatively close to regional S_{Hmax} directions.

4.4. Dynamic Poisson's ratios

Poisson's ratios for five wells (DB102, DB101, DB104, DX1 and TZ4) in the study area vary from *ca.*0 to 0.4776 with average values falling into the range between 0.1448 and 0.3078 (Table 4). The lowest average value of poisson's ratio (0.1448) is found in well DB101 that has a fracture density of 0.031 F/m, while the highest average value of poisson's ratio (0.3078) is found in Well DB 104 with a fracture density of 0.961 F/m (Table 4). Closer inspection indicates that a moderately positive correlation exists between the densities of hinge-parallel fractures and the dynamic poisson's ratios (Fig. 13a). If all fracture sets were

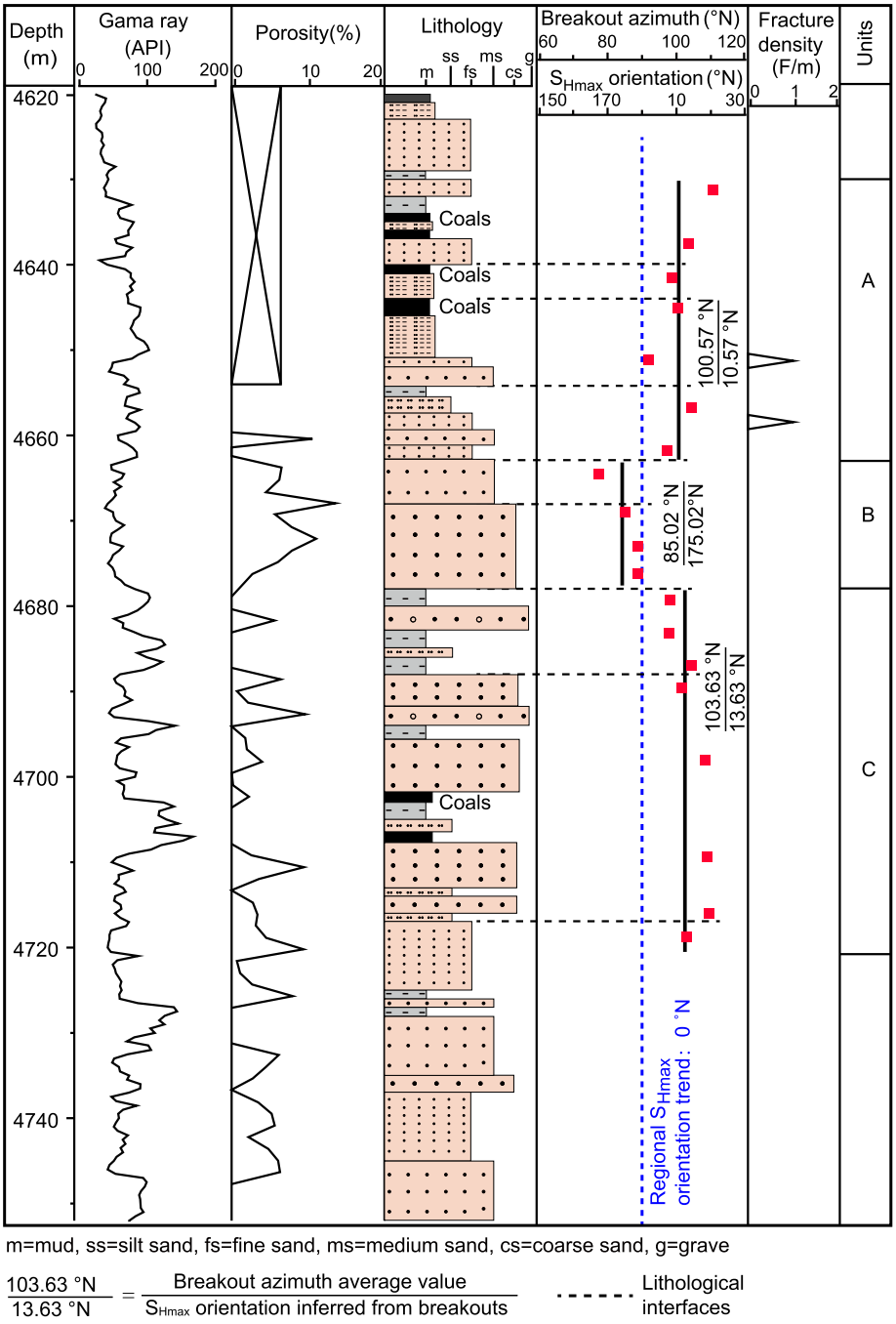

Fig. 10. Lithology, breakout and stress orientations, and porosity profile for well DB103. Lithology is based on cutting logs. Note that stress and borehole breakout orientations are plotted in one column by using the same symbol but different azimuth coordinates. Dashed black lines highlight lithological interfaces that record evident borehole breakout rotation. Heavy black lines represent the average orientations of S_{Hmax} and breakouts for a given unit.

considered, a more distinct positive correlation ($R^2 = 0.71$) is found between the fracture densities and the dynamic poisson's ratios (Fig. 13b).

5. Discussion

5.1. Relationship between fracturing and stress re-orientation

We have recognized plate boundary forces to be the first-order factor controlling stress pattern in the study area. Faults and fractures were identified to have affected local stress orientations against the background of the first-order stress pattern. Depth-dependent stress orientations in poorly-fractured or non-fractured units commonly fluctuate around regional stress orientations, and variations in stress orientations in those units are usually related to lithological changes (Fig. 10; unit D in Fig. 11; units ML3 and ML6 in Fig. 12). Previous studies have identified the vertical change in stress orientations due to lithological variation based on continuous profiles of borehole breakouts (Lin et al., 2010; Talukdar et al., 2022). It is observed here that when lithology varies together with a marked porosity change, evident variation in stress orientations would occur, for example at 4673 m (the interface between units A and B) in well DB103 (Fig. 10) and at 4242.8 m in well TZ4 (Fig. 12).

Previous geological observations have revealed that faulting plays an

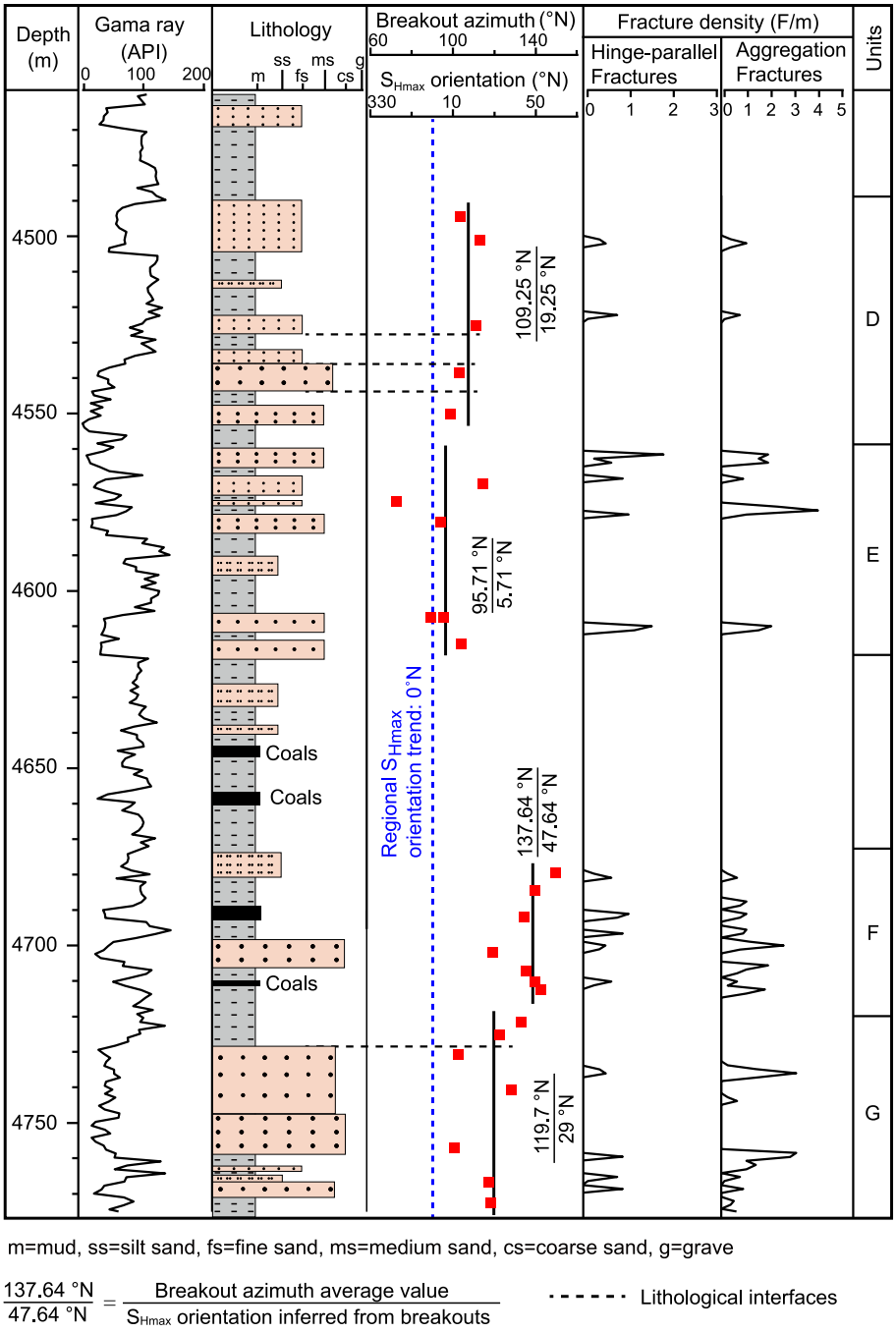

Fig. 11. Lithology, fracture density and breakout orientation profile for well YN2. Captions are the same as Fig. 10.

important role in changing stress orientation (Shamir and Zoback, 1992; Yale, 2003; Tingay et al., 2010; Rajabi et al., 2016b; Radwan et al., 2021; Wang et al., 2022). Such faulting-induced stress rotations or perturbations are considered to be caused by slipping and movement on preexisting faults (Barton and Zoback, 1994) or faulting-induced elastic property contrast between the fault zone and host rock (Gudmundsson et al., 2010; Tingay et al., 2010). Fracturing-related stress reorientation also has been well documented in literatures (Faulkner et al., 2006; Heap et al., 2010; Lin et al., 2010; Rajabi et al., 2016a and b). Faulkner et al. (2006) reported a gradual stress rotation towards the core zone of a strike-slip fault. Such a rotation is related to the change in elastic parameters arising from the development of micro-fractures, which induces a gradual decrease in Young's modulus and a gradual increase in Poisson's ratio as approaching the fault core zone.

Our observation indicates that S_{Hmax} orientations in well fractured wells deviate from the regional stress orientation, with aligning to the strike of NE-striking hinge-oblique fractures, for example wells DB104, TZ4 and DX1 (Fig. 1b, 2c and 4). Poorly-fractured wells (wells YN4, DB101 and DB103), in contrast, commonly display S_{Hmax} orientations roughly consistent with the regional S_{Hmax} orientation (Fig. 1b, 2c and 4). These results confirm that an intimate connection exists between fracturing and local stress variation (Faulkner et al., 2006; Rajabi et al., 2016a and b). Based on fracturing history and stress orientations presented in result section, stress re-orientation occurred after hinge-parallel fracturing but before the formation of NE-striking hinge oblique fractures. Further inspection indicates that the degree rotation of S_{Hmax} orientations (from the regional S_{Hmax} orientation) correlates positively with hinge-parallel fracture densities (with a R^2 of 0.77)

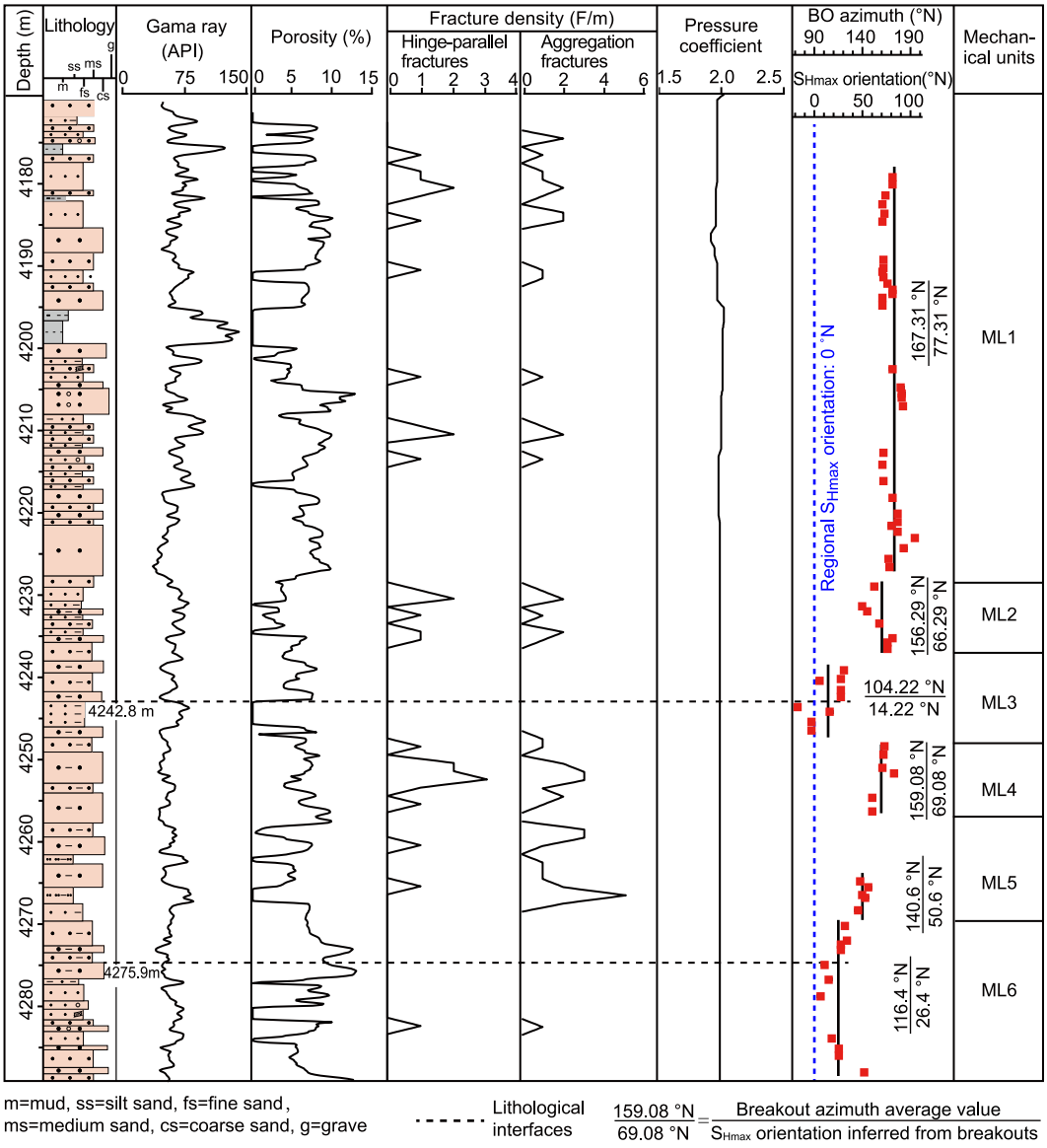

Fig. 12. Composite chart showing lithology, porosity, fracture density, formation pressure coefficient, and borehole breakout and S_{Hmax} orientations for well TZ4. Captions are the same as Fig. 10.

Table 4
Minimum, maximum and average values of poisson's ratios in this study.

Wells	Minimum	Maximum	Average
DB102	0	0.4131	0.2129
DB101	0.0001	0.3786	0.1448
DB104	0.0919	0.4376	0.3078
DX1	0.0003	0.4664	0.2431
TZ4	0.0254	0.4776	0.2114

(Fig. 14). Moreover, nearly all fractures in the present study are open fractures (Fig. 5), which and related micro-fractures can have strong impact on the elastic properties of strata. The moderate to distinct positive correlations between the dynamic poisson's ratio and the fracture density observed in the present study demonstrate that fracturing play an important role in changing lateral elastic parameters and differential fracturing can considerably enhance the geomechanical heterogeneity of strata (Fig. 13).

We thus prefer the interpretation that differential hinge-parallel fracturing likely accounted for the stress rotation, and a conceptual model was developed to illustrate the relationship between fracturing and stress orientations (Fig. 15). During the pre-folding stage, NE- and NW-striking fractures formed across the study area with S_{Hmax} in the S–N direction and consistent with regional stress trend (Fig. 15a). W-E striking faults, fault-related folds and hinge-parallel fractures formed during the syn-folding stage (Yu et al., 2016). A fault and fracture-damaged zone accordingly existed in wells YN2, DB104, DX1 and TZ4 that underwent intense hinge-parallel fracturing (E-W striking) (Fig. 15b). The zone is perpendicular to the regional S_{Hmax} trend, and is mechanically weak and soft enough with respect to less-fractured regions (wells YN4, DB101, DB103 and DB102) to change the S_{Hmax} orientation (Fig. 15c). The NE-striking hinge-oblique fractures were formed in the damaged zone as a response to the stress re-orientation (Fig. 15d). A moderate correlation between densities of hinge-parallel fractures and NE-striking hinge-oblique fractures probably reveal the underlying relationship between the two fracture sets linked by local stress re-orientation (Fig. 6b).

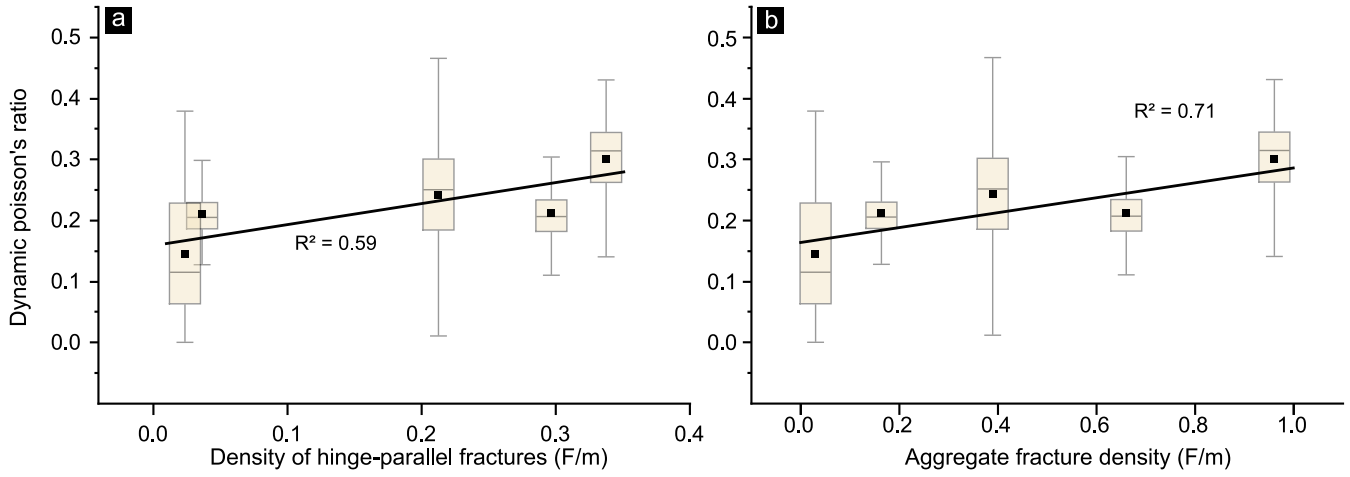

Fig. 13. Plots showing lateral variation (between wells) of elastic parameters owing to fracture development. (a) Density of hinge-parallel fractures and dynamic poisson's ratio show a positive correlation; (b) A obvious positive correlation exists between aggregate fracture density and poisson's ratio with R^2 of 0.71.

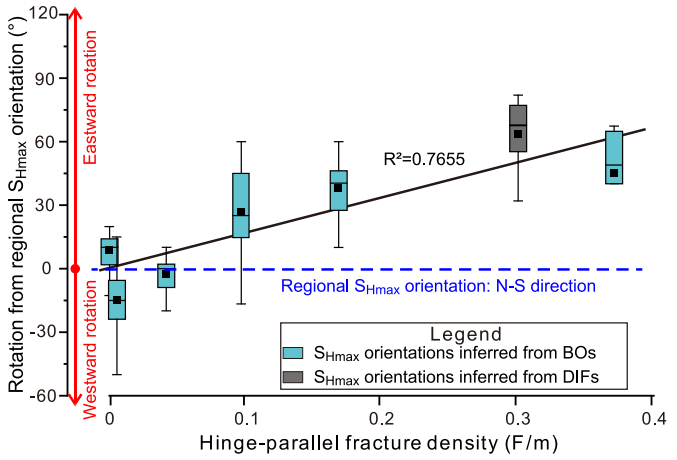

Fig. 14. A plot of hinge-parallel fracture densities and the rotation of S_{Hmax} orientations (from the regional S_{Hmax} orientation) showing a positive correlation with R^2 of 0.77. Note that only S_{Hmax} orientations with A to C quality ranks were used in the plot.

5.2. *Implications for petroleum production and fracture development*

Previous studies revealed that natural fractures can have a crucial role in improving the quality of reservoirs and enhancing fluid flow and petroleum production (Lu et al., 2016; Ju and Wang, 2018; Zhang et al., 2022; Marghani et al., 2023). Fractures in the Jurassic reservoir from Dibei-Tuziluoke Gas Field have been considered to be favorable for the formation of sweet spots that are characterized by relatively higher porosity and permeability and beneficial to petroleum migration and accumulation (Jiang et al., 2015; Lu et al., 2016). Fractures also enhance petroleum production significantly, especially those that are aligned with the *in situ* S_{Hmax} orientation (Ju and Wang, 2018). Our results indicate that the coupling of fracturing (faulting) and stress orientation has produced fracture swarms in wells DB104, TZ4, DX1 and YN2 (Fig. 15d). These fracture swarms may have significantly enhanced subsurface fluid flow. Available production data indicates that wells drilled into fracture swarms are commonly characterized by high gas production rate. For example, wells DB104, DX1 and YN2 produce gas at rates of 780×10^3, 660×10^3 and 109×10^3 m^3/d, respectively (Fig. 2c and 16). In contrast, wells drilled outside the fracture swarms (wells YN4, DB102, DB103 and DB101) have low or almost no gas production. Well TZ4 (located in the Tuziluoke Gas Field), being characterized by a high fracture density but very low gas production rate, seems to be an exception to the general rule. This is because gas in the Tuziluoke Gas Field was generated in the Triassic and Jurassic source rocks, having migrated upwards via faults and the fractured Jurassic reservoir interval to accumulate in the upper Neogene sandstones (Wang et al., 2016). Our fracture and gas production rate data for the well were actually measured for the Jurassic sandstone reservoir and there are no image logs available for the Neogene strata.

Multiple geological factors have been well documented to influence fracture distribution and patterns including structural position (Stearns, 1968; Hanks et al., 1997; Ghosh and Mitra, 2009; Watkins et al., 2015), sedimentary architecture (Zahm and Hennings, 2009; Ogata et al., 2017), distance to faults (Gudmundsson et al., 2010; Wang et al., 2021), diagenesis (Shackleton et al., 2005; Hooker and Katz, 2015) and bed thickness (Wennberg et al., 2006; Sonntag et al., 2012) *etc*. It also has been well documented that how natural fractures couple with in-situ stress and how fault-related local stress perturbations influence fracture patterns (Rawnsley et al., 1998; Gudmundsson et al., 2010; Maerten et al., 2018; Cui and Radwan, 2022). The study in the Dibei-Tuziluoke Gas Field in the Kuqa Foreland Basin has confirmed that geomechanical heterogeneities related to fracturing are a major factor affecting local stress orientations on a scale of several kilometers. Our observation regarding the relationship between fracturing and stress orientation in the Kuqa Foreland Basin demonstrates that pre-existing fractures or faults can influence subsequent fracturing by altering the local stress field.

These results should help us to better understand fracture patterns and predication. Firstly, fracturing or faulting-related stress reorientation is quite common in sedimentary basins (Rawnsley et al., 1998; Tingay et al., 2010; Rajabi et al., 2016b; Wang et al., 2022), any simple and arbitrary assumptions that S_{Hmax} orientation is consistent with regional trend or remains unchanged thus may not be correct. It is suggested here that the linkage between fracturing and stress orientation should be incorporated into fracture characterization and numerical modeling to gain a reliable fracture predication output. Secondly, depth-dependent variations of borehole breakouts indicate that S_{Hmax} orientations for well-fractured intervals usually deviate from the regional stress trend significantly, while poorly-fractured intervals typically have S_{Hmax} orientations consistent with the regional stress trend. Vertical variations of S_{Hmax} orientations owing to the differential fracturing may result in decoupling of adjacent mechanical layers and thus complicate fracture stratigraphy.

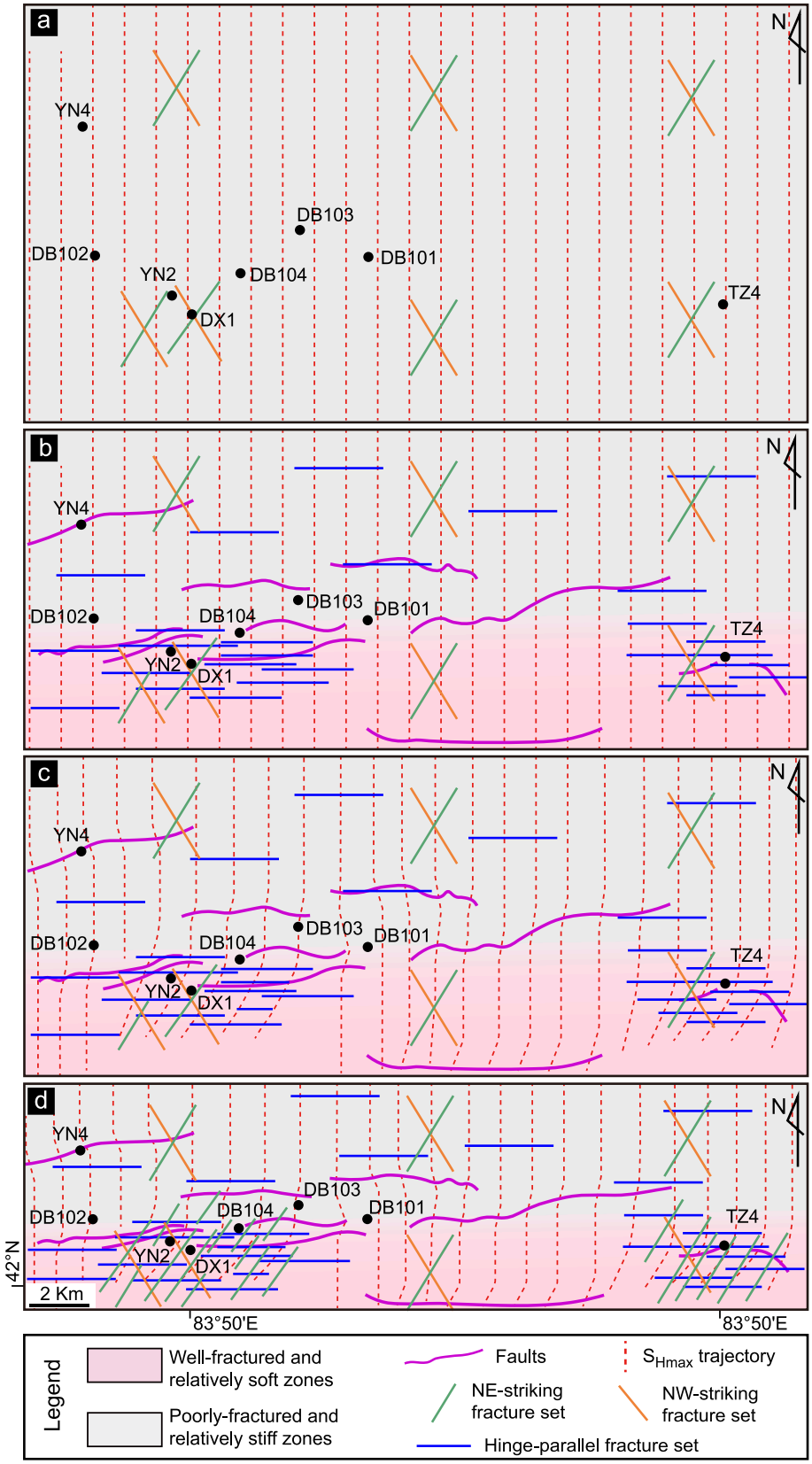

Fig. 15. Conceptual model illustrating relationships between faulting or fracturing and local stress orientation. (a) Pre-folding stage. NE- and NW-striking hinge-oblique fractures formed as a conjugate fracture set with S_{Hmax} orientations in north-south direction; (b) Syn-folding stage. An EW-trending damaged zone occurred in wells YN2, DB104, DX1 and TZ4 because of intense hinge-parallel faulting or fracturing. (c) The zone is perpendicular to the regional S_{Hmax} trend and mechanically weak enough with respect to less-fractured regions (wells YN4, DB101, DB102 and DB103) to deflect the S_{Hmax} orientation; (d) Post-folding stage. NE-striking hinge-oblique fractures formed in the re-oriented stress system. Note that hinge-normal fractures were not included here; following Yu et al. (2016), this fracture set was interpreted to form during post-folding stage but before stress reorientation.

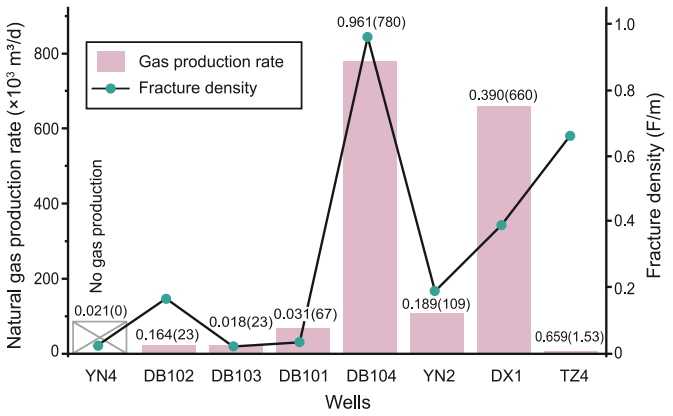

Fig. 16. Bar chart showing fracture densities and gas production rates in the Dibei-Tuziluoke Gas Field. The numbers next to bars denote fracture densities with gas production rate in brackets.

5.3. Limitations of this study

Despite of the promising results presented in this study, there are some limitations. Firstly, although we have confirmed that fracturing can significantly alter elastic properties of strata by using logging data, it is worth noting that other factors including lithology, diagenesis and porosity may also have effect on the elastic properties of rocks. No effort was made to analyze the influence of these factors on elastic properties. Secondly, we have revealed the relationship between fracturing and stress orientation only based on geological observations. The results would be more convincing and compelling if they are backed up by numerical modeling.

6. Conclusions

Through a systematic investigation of subsurface fractures and *in-situ* stress orientations in the Dibei-Tuziluoke Gas field along an E-W striking fold thrust in the Kuqa Foreland Basin, we have characterized lateral (between wells) and depth-dependent variations of S_{Hmax} orientations and revealed that faults and fractures are major factors controlling stress re-orientation on a scale of several kilometers, and that pre-existing fractures or faults can influence subsequent fracture patterns to produce fracture swarms by affecting local stress orientations.

(1) Our study area is dominated by two fracture sets: hinge-parallel fractures and NE-striking hinge oblique fractures. The *in-situ* orientations of the maximum horizontal stress (S_{Hmax}) derived from borehole breakouts and drilling-induced fractures for eight wells are highly variable and occur as two different stress patterns: 1) NNW and NNE (165.08 and 188.59 °N), and 2) NNE to ENE (26.65–57.77 °N).

(2) The first stress pattern has S_{Hmax} orientations that are roughly consistent with the regional stress field inferred from earthquake focal mechanism solutions in northwestern China from WSM. The stress pattern is thus interpreted to be regionally controlled by plate boundary forces generated from the collision between the Indian and Eurasian plates. The second stress pattern is parallel or sub-parallel to the NE-striking hinge oblique fractures and is incompatible with regional stress trend.

(3) Depth-dependent S_{Hmax} orientations also exhibit evident variations. Well-fractured intervals normally display stress orientations that deviate from the regional stress pattern. In contrast, the overall S_{Hmax} orientations for slightly or poorly-fractured intervals are generally consistent with the regional stress trend, although there are widespread variations in depth-dependent stress orientation associated with lithological changes.

(4) Faults and hinge-parallel fractures (E-W striking) formed during syn-folding probably resulted in heterogeneity of elastic parameters, which deflected S_{Hmax} from the regional trend to NNE–ENE directions, both laterally and vertically, generating a new stress pattern (the second stress pattern). NE-striking hinge-oblique fractures were developed in the rotated stress system. The coupling between fracturing and stress orientation can produce fracture swarms, which significantly enhance fluid flow and petroleum production.

Declaration of competing interest

The authors declare that they have no known competing financial interests or personal relationships that could have appeared to influence the work reported in this paper.

Data availability

The data that has been used is confidential.

Acknowledgements

This work was jointly supported by PetroChina Major Research Program on Deep Petroleum System in the Tarim Basin (No. ZD2019-183-01-003), the Major Research Project on the Tethys Geodynamic System from the National Natural Science Foundation of China (No. 92055204) and National Natural Science Foundation of China (No. 42072134). The Tarim Oilfield Company, PetroChina is thanked for providing basic data used in this paper. We are grateful to the associate editor, Dr Alexander L Peace, and five anonymous reviewers for their constructive comments and suggestions on our manuscript.

References

Aadnoy, B.S., Bell, J.S., 1998. Classification of drill-induce fractures and their relationship to in-situ stress directions. Log. Anal. 39, 27–42.
Alexeiev, D.V., Biske, Y.S., Wang, B., Djenchuraeva, A.V., Getman, O.F., Aristov, V.A., Kröner, A., Liu, H.S., Zhong, L.L., 2015. Tectono-stratigraphic framework and Palaeozoic evolution of the Chinese south Tianshan. Geotectonics 49, 93–122.
Ameen, M.S., 2016. Fracture modes in the Silurian Qusaiba shale play, northern Saudi Arabia and their geomechanical implications. Mar. Petrol. Geol. 78, 312–355.
Baouche, R., Sen, S., Sadaoui, M., Boutaleb, K., Ganguli, S.S., 2020. Characterization of pore pressure, fracture pressure, shear failure and its implications for drilling, wellbore stability and completion design — a case study from the Takouazet field, Illizi Basin, Algeria. Mar. Petrol. Geol. 120, 104510.
Baouche, R., Sen, S., Chaouchi, R., Ganguli, S.S., 2021. Modeling In-situ tectonic stress state and maximum horizontal stress azimuth in the Central Algerian Sahara–A geomechanical study from El Agreb, El Gassi and Hassi Messaoud fields. J. Nat. Gas Sci. Eng. 88, 103831.
Barton, C.A., Zoback, M.D., 1994. Stress perturbations associated with active faults penetrated by boreholes: Possible evidence for near-complete stress drop and a new technique for stress magnitude measurement. J. Geophys. Res. Solid Earth 99 (B5), 9373–9390.
Barton, C.A., Zoback, M.D., Moos, D., 1995. Fluid flow along potentially active faults in crystalline rock. Geology 23 (8), 683–686.
Beaumont, E.A., Foster, N.H., 1999. Exploring for Oil and Gas Traps. The American Association of Petroleum Geologists, Oklahoma.
Bell, J., 1996. Petro geoscience 2. In situ stresses in sedimentary rocks (part 2): applications of stress measurements. Geosci. Can. 23, 135–153.
Bell, J.S., Gough, D.I., 1979. Northeast-southwest compressive stress in Alberta evidence from oil wells. Earth Planet Sci. Lett. 45 (2), 475–482.
Brudy, M., Zoback, M., 1999. Drilling-induced tensile wall-fractures: implications for determination of in-situ stress orientation and magnitude. Int. J. Rock Mech. Min. Sci. 36 (2), 191–215.
Charvet, J., Shu, L.L., Laurent-Charvet, S., Wang, B., Faure, M., Cluzel, D., Chen, Y., De Jong, K., 2011. Palaeozoic tectonic evolution of the Tianshan belt, NW China. Sci. China Earth Sci. 54 (2), 166–184.
Cui, X.Y., Radwan, A.E., 2022. Coupling relationship between current in-situ stress and natural fractures of continental tight sandstone oil reservoirs. Interpretation 10 (3). SF9–SF21.
Faulkner, D.R., Mitchell, T.M., Healy, D., Heap, M.J., 2006. Slip on 'weak' faults by the rotation of regional stress in the fracture damage zone. Nature 444 (7121), 922–925.
Finkbeiner, T., Barton, C.A., Zoback, M.D., 1997. Relationships among in-situ stress, fractures and faults, and fluid flow: Monterey Formation, Santa Maria Basin, California. AAPG Bull. 81 (12), 1975–1999.
Fossen, H., 2020. Structural Geology, second ed. Cambridge university press, Cambridge.

Ganguli, S.S., Vedanti, N., Pandey, O.P., Dimri, V.P., 2018. Deep thermal regime, temperature induced over-pressured zone and implications for hydrocarbon potential in the Ankleshwar oil field, Cambay basin, India. J. Asian Earth Sci. 161, 93–102.
Ghosh, K., Mitra, S., 2009. Structural controls of fracture orientations, intensity, and connectivity, Teton anticline, Sawtooth Range, Montana. AAPG Bull. 93 (8), 995–1014.
Gudmundsson, A., Simmenes, T.H., Larsen, B., Philipp, S.L., 2010. Effects of internal structure and local stresses on fracture propagation, deflection, and arrest in fault zones. J. Struct. Geol. 32 (11), 1643–1655.
Guo, X.P., Ding, X.Z., He, X.X., Li, H.M., Su, X., Peng, Y., 2002. New progress in the study of marine transgressional events and marine strata of the Meso-Cenozoic in the Tarim Basin. Acta Geol. Sin. 76, 299–307 (In Chinese with English abstract).
Hanks, C.L., Lorenz, J., Teufel, L., Krumhardt, A.P., 1997. Lithologic and structural controls on natural fracture distribution and behavior within the Lisburne Group, northeastern Brooks Range and North Slope subsurface, Alaska. AAPG Bull. 81 (10), 1700–1720.
He, D.F., Zhou, X.Y., Yang, H.J., Lei, G.L., Ma, Y.J., 2009. Geological structure and its controls on giant oil and gas fields in Kuqa depression, Tarim Basin: a clue from new shot seismic data. Geotect. Metallogenia 33 (1), 19–32 (In Chinese with English abstract).
Heap, M.J., Faulkner, D.R., Meredith, P.G., Vinciguerra, S., 2010. Elastic moduli evolution and accompanying stress changes with increasing crack damage: implications for stress changes around fault zones and volcanoes during deformation. Geophys. J. Int. 183 (1), 225–236.
Heidbach, O., Rajabi, M., Reiter, K., Ziegler, M., 2016. World Stress Map 2016. GFZ Data Service. https://doi.org/10.5880/WSM.2016.002.
Heidbach, O., Tingay, M., Barth, A., Reinecker, J., Kurfeß, D., Müller, B., 2010. Global crustal stress pattern based on the World Stress Map database release 2008. Tectonophysics 482 (1–4), 3–15.
Hendrix, M.S., Graham, S.A., Carroll, A.R., Sobel, E.R., Mcknight, C.L., Schulein, B.J., Wang, Z.X., 1992. Sedimentary record and climatic implications of recurrent deformation in the Tian Shan: evidence from Mesozoic strata of the north Tarim, south Junggar, and Turpan basins, northwest China. Geol. Soc. Am. Bull. 104 (1), 53–79.
Hooker, J.N., Katz, R.F., 2015. Vein spacing in extending, layered rock: the effect of synkinematic cementation. Am. J. Sci. 315 (6), 557–588.
Hu, X.M., Garzanti, E., Moore, T., Raffi, I., 2015. Direct stratigraphic dating of India-Asia collision onset at the Selandian (middle Paleocene, 59±1 Ma). Geology 43 (10), 859–862.
Hu, X.P., Zang, A., Heidbach, O., Cui, X.F., Xie, F.R., Chen, J.W., 2017. Crustal stress pattern in China and its adjacent areas. J. Asian Earth Sci. 149, 20–28.
Jia, C.Z., 2004. Characteristics of Mesozoic and Cenozoic Structures and Petroleum Occurrence in the Tarim Basin. Petroleum Industry Press, Beijing (in Chinese).
Jia, C.Z., 2013. Characteristics of Chinese Petroleum Geology: Geological Features and Exploration Cases of Stratigraphic, Foreland and Deep Formation Traps. Springer-Verlag, Hangzhou; Berlin Heidelberg. Zhejiang University Press.
Jiang, Z.X., Li, F., Yang, H.J., Li, Z., Liu, L.F., Chen, L., Du, Z.M., 2015. Development characteristics of fractures in Jurassic tight reservoir in Dibei area of Kuqa depression and its reservoir-controlling mode. Acta Pet. Sin. 36, 102–111 (In Chinese with English abstract).
Jolivet, M., Heilbronn, G., Robin, C., Barrier, L., Bourquin, S., Guo, Z., Jia, Y., Guerit, L., Yang, W., Fu, B., 2013. Reconstructing the Late Palaeozoic–Mesozoic topographic evolution of the Chinese Tian Shan: available data and remaining uncertainties. Adv. Geosci. 37, 7–18.
Ju, W., Wang, K., 2018. A preliminary study of the present-day in-situ stress state in the Ahe tight gas reservoir, Dibei Gas field, Kuqa Depression. Mar. Petrol. Geol. 96, 154–165.
Ju, W., Hou, G.T., Huang, S.Y., Ren, K.X., 2013. Structural fracture distribution and prediction of the lower Jurassic Ahe Formation sandstone in the Yinan-Tuzi area, Kuqa depression. Geotect. Metallogenia 37 (4), 592–602 (In Chinese with English abstract).
Ju, W., Wang, K., Hou, G.T., Sun, W.F., Yu, X., 2018. Prediction of natural fractures in the lower Jurassic Ahe Formation of the Dibei gas field, Kuqa depression, Tarim Basin, NW China. Geosci. J. 22 (2), 241–252.
Khoshbakht, F., Memarian, H., Mohammadnia, M., 2009. Comparison of Asmari, Pabdeh and Gurpi formation's fractures, derived from image log. J. Petrol. Sci. Eng. 67 (1–2), 65–74.
Lai, J., Wang, G.W., Wang, S., Cao, J.T., Li, M., Pang, X.J., Han, C., Fan, X.Q., Liu, Yang, He, Z.B., Qin, Z.Q., 2018. A review on the applications of image logs in structural analysis and sedimentary characterization. Mar. Petrol. Geol. 95, 139–166.
Lai, J., Wang, G.W., Fan, Q.X., Pang, X.J., Li, H.B., Zhao, F., Li, Y.H., Zhao, X., Zhao, Y.D., Huang, Y.Y., Bao, M., Qin, Z.Q., Wang, Q.Q., 2022. Geophysical well-log evaluation in the era of unconventional hydrocarbon resources: a review on current status and prospects. Surv. Geophys. 43 (3), 913–957.
Li, J.F., Zhao, Y., Pei, J.L., Liu, F., Zhou, Z.Z., Gao, H.L., Gao, L., Fu, Z.B., 2017. Cenozoic marine sedimentation problem of the Tarim Basin. J. Geomechanics 23 (1), 141–149 (In Chinese with English abstract).
Li, W.F., Wang, C.S., Gao, Z.Z., Peng, D.T., 2000. Sedimentary evolution of Mesozoic era in Kuche depression, Tarim Basin. Acta Sedimentol. Sin. 18 (4), 534–538 (In Chinese with English abstract).
Li, Z., Song, W.J., Peng, S.T., Wang, D.X., Zhang, Z.P., 2004. Mesozoic–Cenozoic tectonic relationships between the Kuqa subbasin and Tian Shan, northwest China: constraints from depositional records. Sediment. Geol. 172 (3–4), 223–249.
Lin, W.R., Yeh, E.C., Hung, J.H., Haimson, B., Hirono, T., 2010. Localized rotation of principal stress around faults and fractures determined from borehole breakouts in hole B of the Taiwan Chelungpu-fault Drilling Project (TCDP). Tectonophysics 482 (1–4), 82–91.
Liu, C.L., Cao, Y.T., Yang, H.J., Jiao, P.C., Gu, Q.Y., 2013. Discussion on Paleogene-Neogene environmental change of salt lakes in Kuqa Foreland Basin and its potash-forming effect. Acta Geosci. Sin. 34, 547–558 (In Chinese with English abstract).
Liu, J.L., Jiang, Z.X., Liu, K.Y., Gui, L.L., Xing, J.Y., 2016. Hydrocarbon sources and charge history in the southern slope region, Kuqa foreland basin, northwestern China. Mar. Petrol. Geol. 74, 26–46.
Lorenz, J.C., Cooper, S.P., 2020. Applied Concepts in Fractured Reservoirs. John Wiley and Sons Ltd, West Sussex.
Lu, H., Lu, X.S., Fan, J.J., Zhao, M.J., Wei, H.X., Zhang, B.S., Lu, Y.H., 2016. Controlling effect of fractures on gas accumulation and production within the tight sandstone: a case study on the Jurassic Dibei gas reservoir in the eastern part of the Kuqa foreland basin, China. Journal of Natural Gas Geoscience 1 (1), 61–71.
Lu, H.F., Chen, C.M., Liu, Z.H., Jia, D., Wang, G.Q., Jia, C.Z., 2000. The structural features and origin of the Kuqa rejuvenation foreland thrust belt. Acta Pet. Sin. 21 (3), 18–24 (In Chinese with English abstract).
Maerten, L., Maerten, F., Lejri, M., 2018. Along fault friction and fluid pressure effects on the spatial distribution of fault-related fractures. J. Struct. Geol. 108, 198–212.
Marghani, M.M., Zairi, M., Radwan, A.E., 2023. Facies analysis, diagenesis, and petrophysical controls on the reservoir quality of the low porosity fluvial sandstone of the Nubian formation, east Sirt Basin, Libya: Insights into the role of fractures in fluid migration, fluid flow, and enhancing the permeability of low porous reservoirs. Mar. Petrol. Geol. 147, 105986.
Molnar, P., Tapponnier, P., 1975. Cenozoic tectonics of Asia: effects of continental collision. Science 189, 419–426.
Morin, J., Jolivet, M., Barrier, L., Laborde, A., Li, H., Dauteuil, O., 2019. Planation surfaces of the tian Shan range (Central Asia): Insight on several 100 million years of topographic evolution. J. Asian Earth Sci. 177, 52–65.
Nian, T., Wang, G.W., Xiao, C.W., Zhou, L., Deng, L., Li, R.J., 2016. The in situ stress determination from borehole image logs in the Kuqa Depression. J. Nat. Gas Sci. Eng. 34, 1077–1084.
Ogata, K., Storti, F., Balsamo, F., Tinterri, R., Bedogni, E., Fetter, M., Hatushika, R., 2017. Sedimentary facies control on mechanical and fracture stratigraphy in turbidites. Geol. Soc. Am. Bull. 129 (1–2), 76–92.
Rawnsley, K.D., Peacock, D.C.P., Rives, T., Petit, J.P., 1998. Joints in the Mesozoic sediments around the Bristol channel basin. J. Struct. Geol. 20 (12), 1641–1661.
Rajabi, M., Sherkati, S., Bohloli, B., Tingay, M., 2010. Subsurface fracture analysis and determination of in-situ stress direction using FMI logs: an example from the Santonian carbonates (Ilam Formation) in the Abadan Plain, Iran. Tectonophysics 492 (1–4), 192–200.
Rajabi, M., Tingay, M., Heidbach, O., 2016a. The present-day stress field of New South Wales, Australia. Aust. J. Earth Sci. 63 (1), 1–21.
Rajabi, M., Tingay, M., King, R., Heidbach, O., 2016b. Present-day stress orientation in the Clarence-Moreton Basin of New South Wales, Australia: a new high density dataset reveals local stress rotations. Basin Res. 29, 622–640. https://doi.org/10.1111/bre.12175.
Radwan, A.E., Abdelghany, W.K., Elkhawaga, M.A., 2021. Present-day in-situ stresses in Southern Gulf of Suez, Egypt: Insights for stress rotation in an extensional rift basin. J. Struct. Geol. 147, 104334.
Shackleton, J.R., Cooke, M.L., Sussman, A.J., 2005. Evidence for temporally changing mechanical stratigraphy and effects on joint-network architecture. Geology 33 (2), 101–104.
Shamir, G., Zoback, M.D., 1992. Stress orientation profile to 3.5 km depth near the San Andreas fault at Cajon Pass, California. J. Geophys. Res. Solid Earth 97 (B4), 5059–5080.
Sonntag, R., Evans, J.P., Pointe, P.L., Deraps, M., Sisley, H., Richey, D., 2012. Sedimentological controls on the fracture distribution and network development in Mesaverde Group sandstone lithofacies, Uinta Basin, Utah, USA. In: Spence, G.H., Redfern, J., Aguilera, R., Bevant, T.G., Cosgrove, J.W., Daniel, J.M. (Eds.), Advances in the Study of Fractured Reservoirs, vol. 374. Geological society, London, Special Publication, pp. 23–50.
Stearns, D.W., 1968. Certain aspects of fracture in naturally deformed rocks. In: Riecker, R.E. (Ed.), NSF Advanced Science Seminar in Rock Mechanics, vol. 1. Air Force Cambridge Research Laboratories, Bedford, Massachusetts, pp. 97–116.
Sun, S., Hou, G.T., Zheng, C.F., 2017. Fracture zones constrained by neutral surfaces in a fault-related fold: Insights from the Kelasu tectonic zone, Kuqa Depression. J. Struct. Geol. 104, 112–124.
Talukdar, M., Sone, H., Kuo, L.W., 2022. Lithology and fault-related stress variations along the TCDP boreholes: the stress state before and after the 1999 Chi-Chi earthquake. J. Geophys. Res. Solid Earth 127 (2), e2021JB023290. https://doi.org/10.1029/2021JB023290.
Tapponnier, P., Molnar, P., 1979. Active faulting and Cenozoic tectonics of the Tien Shan, Mongolia, and baykal regions. J. Geophys. Res. Solid Earth 84, 3425–3459.
Tingay, M., Reinecker, J., Müller, B., 2008. Borehole breakout and drilling-induced fracture analysis from image logs. World Stress Map Project 1–8. Guidelines: Image logs.
Tingay, M.R., Morley, C.K., Hillis, R.R., Meyer, J., 2010. Present-day stress orientation in Thailand's basins. J. Struct. Geol. 32 (2), 235–248.
Wang, J.P., Zeng, L.B., Yang, X.Z., Liu, C., Wang, K., Zhang, R.H., Chen, X.G., Qu, Y.J., Laubach, S.E., Wang, Q.Q., 2021. Fold-related fracture distribution in Neogene, Triassic, and Jurassic sandstone Outcrops, northern Margin of the Tarim Basin, China: Guides to deformation in Ultradeep tight sandstone reservoirs. Lithosphere 2021 (Special 1), 8330561. https://doi.org/10.2113/2021/8330561.
Wang, K., Zhang, R.H., Yu, C.F., Yang, Z., Tang, Y.G., Wei, H.X., 2020. Characteristics and controlling factors of Jurassic Ahe reservoir of the northern tectonic belt, Kuqa

depression, Tarim Basin. Nat. Gas Geosci. 31 (5), 623–635 (In Chinese with English abstract).
Wang, S., Wang, G.W., Li, D., Wu, X.N., Chen, X., Wang, Q.Q., C, J.T., Zhang, Y.L., 2022. Comparison between double caliper, imaging logs, and array sonic log for determining the in-situ stress direction: a case study from the ultra-deep fractured tight sandstone reservoirs, the Cretaceous Bashijiqike Formation in Keshen 8 region of Kuqa depression, Tarim Basin, China. Petrol. Sci. 19 (6), 2601–2617.
Wang, X., Wei, H.X., Shi, W.Z., Wang, Y., 2016. Characteristics of formation pressure and its relationship with hydrocarbon accumulation in the eastern part of Kuqa Depression. Geol. Sci. Technol. Inf. 35 (1), 68–73.
Watkins, H., Butler, R.W., Bond, C.E., Healy, D., 2015. Influence of structural position on fracture networks in the Torridon Group, Achnashellach fold and thrust belt, NW Scotland. J. Struct. Geol. 74, 64–80.
Wennberg, O.P., Svånå, T., Azizzadeh, M., Aqrawi, A.M.M., Brockbank, P., Lyslo, K.B., Ogilvie, S., 2006. Fracture intensity vs. mechanical stratigraphy in platform top carbonates: the Aquitanian of the Asmari formation, Khaviz anticline, Zagros, SW Iran. Petrol. Geosci. 12 (3), 235–246.
Xiao, W.J., Windley, B.F., Allen, M.B., Han, C.M., 2013. Paleozoic multiple accretionary and collisional tectonics of the Chinese Tianshan orogenic collage. Gondwana Res. 23 (4), 1316–1341.
Yale, D.P., 2003. Fault and stress magnitude controls on variations in the orientation of in situ stress. In: Ameen, M. (Ed.), Fracture and In-Stiu Stress Characterization of Hydrocarbon Reservoirs. Geological Society, London, Special Publication 209, pp. 55–64.
Yu, X., Hou, G.T., Neng, Y., Li, J., Wei, H.X., 2016. Development and distribution characteristics of tectonic fractures in Kuqa depression. Geol. J. China Univ. 22 (4), 644–656 (In Chinese with English abstract).
Zahm, C.K., Hennings, P.H., 2009. Complex fracture development related to stratigraphic architecture: Challenges for structural deformation prediction, Tensleep Sandstone at the Alcova anticline, Wyoming. AAPG Bull. 93 (11), 1427–1446.
Zeng, L.B., Wang, H.J., Gong, L., Liu, B.M., 2010. Impacts of the tectonic stress field on natural gas migration and accumulation: a case study of the Kuqa Depression in the Tarim Basin, China. Mar. Petrol. Geol. 27 (7), 1616–1627.
Zhan, Y., Hou, G.T., Sun, X.W., Ju, W., Shen, Y.M., Zhao, W.T., Ren, X.K., Zhang, P., 2014. Quantitative prediction of tectonic fractures of Jurassic sandstones in the eastern Kuche depression. Geol. J. China Univ. 20 (2), 294–302 (In Chinese with English abstract).
Zhang, Q., Wu, X.S., Radwan, A.E., Wang, B.H., Wang, K., Tian, H.Y., Yin, S., 2022. Diagenesis of continental tight sandstone and its control on reservoir quality: a case study of the Quan 3 member of the cretaceous Quantou Formation, Fuxin uplift, Songliao Basin. Mar. Petrol. Geol. 145, 105833.
Zhang, T., Fang, X.M., Song, C.H., Appel, E., Wang, Y.D., 2014. Cenozoic tectonic deformation and uplift of the South Tian Shan: implications from magnetostratigraphy and balanced cross-section restoration of the Kuqa depression. Tectonophysics 628, 172–187.
Zhang, Z.B., Zhao, X.C., Ren, L., 2020. Focal mechanism solution and tectonic stress field characteristics of the middle Tianshan mountains, Xinjiang. Seismol. Geol. 42 (3), 595–611 (In Chinese with English abstract).
Zhang, Y.Z., Dusseault, M.B., Yassir, N.A., 1994. Effects of rock anisotropy and heterogeneity on stress distributions at selected sites in North America. Eng. Geol. 37 (3–4), 181–197.
Zhang, Z.P., Wang, Q.C., 2004. Development of joints and shear fractures in the Kuqa depression and its implication to regional stress field switching. Science in China (Series D) 34 (Suppl. l), 63–73 (In Chinese with English abstract).
Zhu, R.K., Guo, H.L., G, Z.Y., Zhang, L.J., Sun, Y.S., Yang, F., Zhang, B.M., Jiang, Y.Q., 2009. Sequence Stratigraphy, Sedimentary System and Reservoir Characteristics during Mesozoic and Cenozoic in Northern Tarim Basin. Geological Publishing House, Beijing (In Chinese).
Zoback, M.D., Moos, D., Mastin, L., Anderson, R.N., 1985. Well bore breakouts and in situ stress: Journal of Geophysical Research. Solid Earth 90 (B7), 5523–5530.
Zoback, M.L., 1992. First- and second-order patterns of stress in the lithosphere: the World stress map Project. J. Geophys. Res. Solid Earth 97 (B8), 11703–11728.